UNIL | Université de Lausanne
Faculté des géosciences
et de l'environnement

Master of Science in Environmental Geoscience

Land grabbing assessment using satellite imagery: a case study in Romania

Myriam Eggerschwiler

Supervisor : Prof. Grégoire Mariéthoz (IDYST, UNIL)
Expert : Prof. Christian Kull (IGD, UNIL)

Cover picture by Karel Nicolas

Landsat 8 false colour image (bands 6 5 4) and its digital number

Acknowledgements

This Master thesis would not have been possible without the guidance and support of many people. I would like to sincerely express my thanks to the following:

- my supervisor, Prof. Grégoire Mariéthoz for his experience and expertise as well as his technical support during this work. I also thank him for the great collaboration we had along this project
- the expert, Prof. Christian Kull for his interest in the project and the time he invested in reading and evaluating this thesis
- my master's program friends for their advices, support and good times we shared together
- my family and my friends who have helped me and were supportive in realizing my goals
- all people who collaborated from near or far to this Master thesis completion.

Abstract

Land grabbing is a worldwide issue that may lead to consequences like environmental damages, exploitation of workers or illegal transactions. Thus, a good understanding of this phenomenon and its actual state is a crucial challenge. We argue that land grabbing implies large-scale land deals and that the evolution of landscape structure and more especially the size of these landscape elements in related to land grabbing. In this Master thesis, land grabbing assessment in Romania, using satellite imagery and remote sensing methods is proposed.

In this work, the proposed methodology consists of four main stages: noise removal, image segmentation, morphological operation and size computation of patches considered as crops. The proposed algorithm is applied on Landsat satellite imagery of 2006 and 2016. The algorithm is implemented and the data acquired using Google Earth Engine, online platform launched in 2010 that provides algorithms and computation skills. Change detection between these years is then obtained and repeated for four different places throughout Romania.

This process reveals that the suggested workflow yield patches considered as crops very close to Landsat image and good results in assessing changes in spatial arrangements of these patches. It also clearly shows an evolution of the sizes of the patches considered as crops over the years with globally a decrease of small-scale patches and increase of large-scale patches. This evolution yield to new insight into land grabbing in Romania.

Patches statistics are finally compared with official Romanian statistics and this comparison reveals that the proposed methodology may lead to some imperfections mainly due the choice of the parameters of the algorithm based on best-fitting visual results. This suggests interesting perspectives for the future, especially thinking about parameters validation and automatic classification.

Table of content

Table of illustrations

I. Introduction

Considerable issues are presently emerging because alimentation is a universal right but food has become a commercial good (Rouillé d'Orfeuil, 2009). The ensuing consequences include environmental damages, exploitation of workers, illegal transactions and land grabbing, amongst others. Indeed, land and the people who take care of it are under considerable threats such as climate change and external pressures. These external pressures can take different forms such as threat of investors or companies seeking land and cannot be ignored. As a matter of fact, as Virgil states (2015, p. 112), *"depuis la convergence des crises multiples au milieu mondiale (financière, environnementale, et alimentaire), il y a eu une réévaluation intense de la terre, suivi d'une vague d'acquisition très importante qui vise principalement les pays du Sud"*. In other words, the growth of the worldwide population and the need for food security, amongst other things, have only highlighted the necessity of investment in land, and thus land that seemed without interest, such as small-scale farming, are now sought after by investors (Borras, Scoones, & Hughes, 2011).

At first glance, these investments could be seen as beneficial to the land and the people it belong to, as the investors claim the various advantages for local work opportunities, green energy production and local food security (Vigil, 2015). On the other hand, these kinds of transactions can put a part of the world's population at great risk. As stated by Zoomers (2010, p. 429), the *"large-scale, cross-border land deals or transactions that are carried out by transnational corporations or initiated by foreign governments"* are usually known as the phenomenon of land grabbing.

Many field trips, local researches, and media stories have addressed the topic of land grabbing and found some evidences of this phenomenon but measuring its scale remains a significant challenge (Franco, Peuch, & Kay, 2015). In practice, these studies are particularly limited by time and costs. Alternatively, analysis of satellite imagery could be a more reliable and cost-effective methodology.

Remote sensing is an interdisciplinary field. It is the science of obtaining information about objects from a distance can improve our understanding of global dynamics and processes like land grabbing that are occurring worldwide or in particular area.

To give a more specific definition, remote sensing is a discipline joining the process of acquisition electromagnetic radiation's energy, the treatment and analysis of such information in order to use the processed data for a given application. It can be used for sea surface temperature monitoring, 3D topography and displacement to prevent natural hazards or urban planning, to list a few uses.

In this work, the aim is to focus on a particular country, Romania, which has seen several political, economic and social changes over the past few years. We put forward the hypothesis that land grabbing implies large-scale land deals and that the evolution of the landscape structure and more specifically the size of these landscape elements is related to land grabbing. The landscape structure consists of patches that are *"specific spatial arrangement of homogeneous landscape elements"* (Brunner, Grêt-Regamey, & Stritih, 2016, p. 10); the homogeneous landscape elements studied in this work are a specific type of crop, assumed to belong to the same exploitation.

Measuring the scale of land grabbing remains, a significant challenge but we argue that it is possible to assess the evolution of those landscape elements. Discriminating crops is complex and we therefore propose a methodology that is based on satellite imagery processing using multiple algorithms. It will provide assessment of changes in the landscape structure combined with estimation of the evolution of the size of patches considered as crops over the years. This work also offers an ideal opportunity to work with Google Earth Engine, a new cloud platform with algorithms and a large amount of freely available images.

II. Context

1. Land grabbing at global scale

In this chapter, an in-depth examination will be given on the global issues. **Figure 1** summarizes the Land Matrix Global Observatory database, which is a global and independent land monitoring initiative mainly based on studies involving fieldwork and local media[1]. This figure shows the global map of investments and the countries targeted by investors from 2000 to 2017 collected by the Land Matrix Global Observatory. It expresses that land grabbing is a global trend that affects many countries throughout the world.

Figure 1. Global map of investments from 2000 to 2017. Targeted countries are displayed (Land Matrix Global Observatory, 2017)

As declared in the introduction, financial and food crisis only increases the need for land acquisitions and this is why the following lines will give an in-depth examination of the global food crisis of 2006-2008. Following Rouillé D'Orfeuil (2009, p. 66), between 2006 and 2008, *"la plupart des prix agricoles et alimentaires ont connu une hausse brutale qui a entrainé une incapacité pour les consommateurs pauvres de s'alimenter convenablement"*. This situation has only strengthened the inequalities leading to food riots in countries like Haiti, Indonesia, Peru, Bolivia, Nigeria or Burkina Faso, amongst others (Dufumier & Hugon, 2008)

[1] See http://www.landmatrix.org/en/

However, as suggested by the Land Matrix Global Observatory database (2017), there was an increase in the number of land deals that were contracted worldwide since 2000. At first sight, these two issues seem to be conflicting because when something like food is abundant the prices are lower. But as a matter of fact, corn, for example, can be grown to be used for food but also biofuels or to feed livestock (Roger-Machart, 2009). In short, the multiple processes that have driven this food crisis were: world population growth, petroleum price increase, biofuels subside and soil and fertility loss amongst others (Bourgeois, 2009). When put back together, trade agreements and agricultural policies are putting small-scale farming under pressure by undoubtedly rising competition to get access to resources like land (Rouillé d'Orfeuil , 2009).

However, historically, these kinds of transactions have no starting date but dispossession of people from their land only emphasizes when political and economic changes emerge. As an example, when 19th century cotton market exploded due to industrial revolution, vast losses in Indian-owned land in the Southeastern of the United States occurred (Magdoff, 2013).

Then, an in-depth investigation will be given on local issues. In fact, with decolonization in the 1960s and increase of nationalizations, in Africa, agribusiness companies started to develop long-term contractual relationships with local suppliers (International land coalition, 2011). This shift from older form of agriculture was made possible for several reasons such as *"economic liberalization, the globalization of transport and communications, and global demand for food*" (Cotula, Keeley, Leonard, & Vermeulen, 2009, p.25).

Moreover, these past few years, several African countries have undergone Chinese requests, for the wheat market, among others, mainly because there was mass increase of the Chinese population between 1952 and 2010 (133 %) (Claverie, 2013). The supply in wheat is fundamental for China and the preservation of an acceptable level of availability is crucial, even for the first world wheat producer. The consumption of wheat has evolved in its form from flour of wheat to leathery meat model but nevertheless the future needs for wheat need to be controlled (Claverie, 2013). Chinese state controls 90 % of the trade but manage and encourage the creation of big firms and the state buys from Chinese peasants as well as importations from global market (Claverie, 2013). Chinese firms such as Cofco, Chinatex Grains and Oils, Sinograin or Beijing Grain rent or buy lands in countries all around the world but mainly in African and Asian countries as it is shown in **Figure 2.**

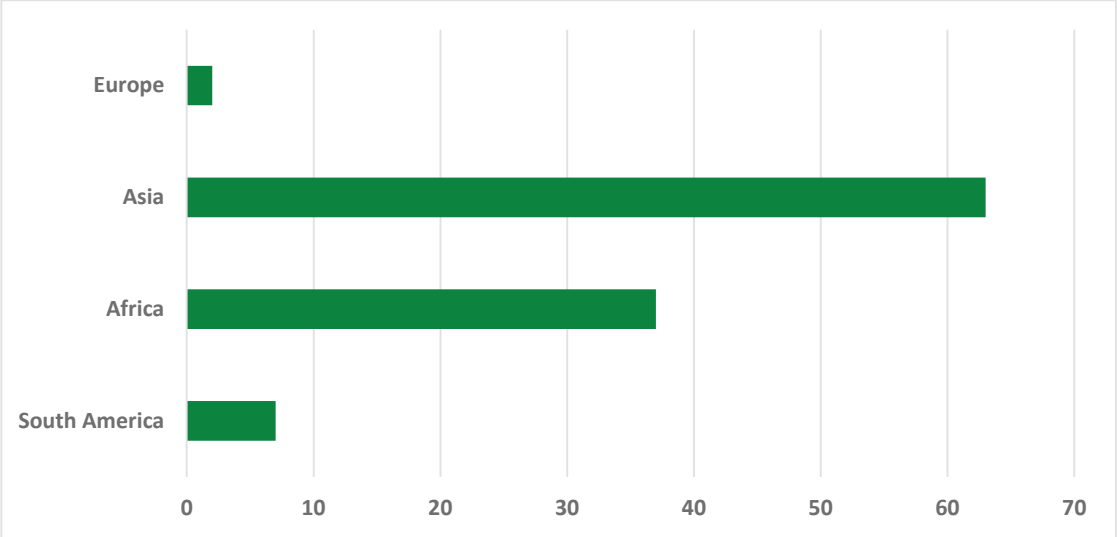

Figure 2. Number of contracted land deals China since 2000 (Land Matrix Global Observatory, 2017)

In short, at a global and local scale, the issues that are behind the land grabbing mechanism are complex. This issue concerns all continents but for that matter, European countries are, for most of them, spared. Actually**, Figure 3** summarizes the number of contracted land deals by countries since 2000. Note that only countries with at least 10 deals concluded were considered. As Asian and African countries are overrepresented, it is interesting to observe that some European countries like Ukraine, Russia or Romania stand out.

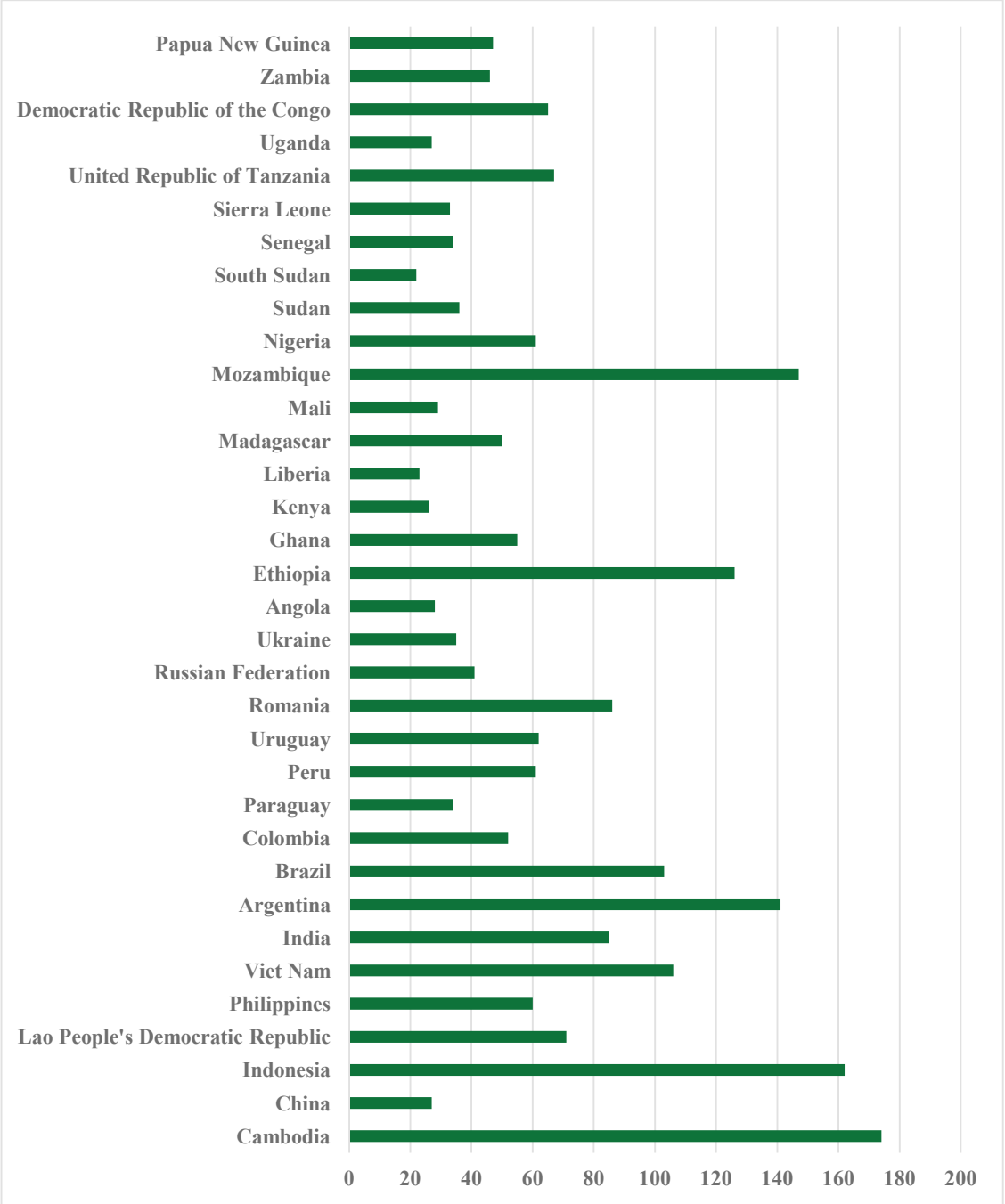

Figure 3. Number of contracted land deals by country since 2000 (Land Matrix Global Observatory, 2017)

So, if undeniably, African and Asian countries have received considerable attention, Post-Soviet countries are nevertheless not spared. Following Spoor and Visser (2011, p. 300), *"only four countries in the world have significant untapped capacity to make a major impact on meeting the growing global food demand, three of which are former Soviet countries, namely Ukraine, Kazakhstan, and Russia while the fourth is Argentina"*.

First of all, the historical background of eastern Europe has its significant importance as decades of Soviet regime has left a heavily subdivided and relatively inefficient agriculture but since the mid-1990, investments have been accelerating and taken an international dimension (Spoor & Visser, 2011). The main processes that drives this acceleration is different from in Africa. The price of the land, the volume of very fertile land that is unused and the quality of infrastructures such as roads and handling networks are some of the factors that make this region very attractive for foreign investors (Spoor & Visser, 2011).

Taking Ukraine as an example: since 2000 and according to the Land Matrix Global Observatory database about 3'650'992 hectares have been allocated to investors. To understand this extent, in Switzerland, in 2015, there were about 1'049'477 hectares of surfaces dedicated to agriculture[2]. Therefore, Ukraine has allocated about 3 times the surface dedicated to agriculture in Switzerland. In terms of losses, this number cannot be neglected and even more when consequences of such process are known. These consequences will be given a closer examination in the following lines.

At first sight, these land allocations could be seen as development opportunities but the impacts cannot be ignored. **Figure 4** enumerates the different impacts of land grabbing on a given country or locality, based on the International Land Coalition report (2012). Nevertheless, governments have seen these lands allocations as favorable because *"investors may bring capital, technology, know-how, infrastructure and market access and may therefore play an important role in catalyzing economic development in rural areas"* (International land coalition, 2011, p. 15)

[2] See LandMatrix.org and https://www.bfs.admin.ch/bfs/fr/home/statistiques/agriculture-sylviculture.assetdetail.268512.html

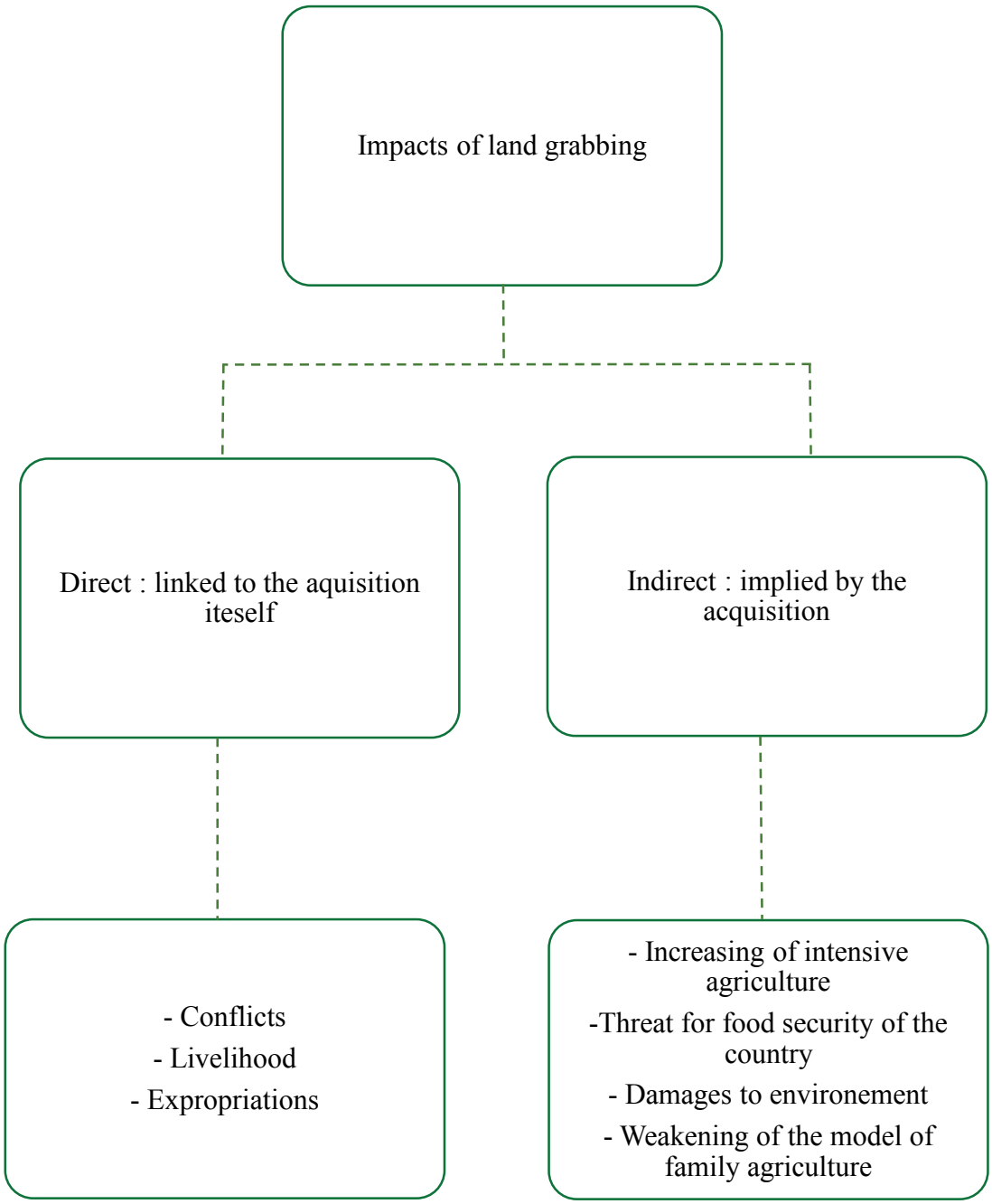

Figure 4. Impacts of land grabbing

2. Going local

Following Franco, Peuch, & Kay (2015, p. 3)*"the rising commercial interest in farmland and the increase in large-scale land deals worldwide"*. Europe is not spared by this phenomenon and according to Franco, Peuch, & Kay (2015, p. 7), *"Evidence indicates that farmland grabbing is concentrated in Eastern European Member states with Poland, Hungary, Bulgaria and Romania emerging as particular hotspots"*. What could be considered as harmless land transactions has nevertheless serious implications for European food security, employment, welfare and biodiversity as well as the demise of small-scale farming. There are various reasons why Romania, who joined the European Union in 2005, has attracted many land investors: for example, relatively low land prices compared to Western Europe and Post-Communist land privatization, which has led to a highly concentrated and highly fragmented land (Kay, 2016). Indeed, changes in agricultural policies and in the criteria for the granting of land can be determinants in the reorganization of agricultural surfaces, which are sometimes accompanied by a change in the use of the soil (Hoster, Kuemmerle, St-Louis, & Radeloff, 2009)

This country has still a very high percentage of the population who are peasants (Knight, 2010). Its farmland history has undertaken several changes but has led to a dichotomy. On the one hand, small-scale farming and on the other hand large agribusiness farms (Knight, 2010)

First, after the First World War, Transylvania was obtained from Hungary and Romania, according to (Knight, 2010, p. 3) , *"Became one of the largest agricultural countries in Europe"*. Then, during the period going from 1948 to 1989, the agricultural lands were collectivized and a lot of agricultural knowledge was lost because a large part of the population moved into urban area (Knight, 2010). In the 1990s, the country switched to a capitalist system and many of the state farms were privatized but these same farms received direct support and subsidies from the government (Knight, 2010). Changes have once more affected peasants in Romania, as the country is a member of the European Union since 2004. The opening of markets to agricultural investment foreigners (laws 312/2005 and 247/2005) as early as 2005 and the implementation of the CAP (Common Agricultural Policy of the EU) in 2007 have been the decisive changes.

The Common agricultural policy (CAP) was born in 1962 short after that the treaty of Rome was signed, politician and people remembering the starvation post to the Second World War. There were different CAP generations, but today it ensures the food security of Europe according to specific needs of each EU country like Romania: *"Europeans Union's farm policy ensures a decent standard of living from farmers, at the same time as setting requirement for animal health and welfare, environmental protection and food safety"* (European commission's directorate

general for agriculture and rural development, 2017). Romania joining the CAP is one of the reasons why many changes happened in this country these past 10 years.

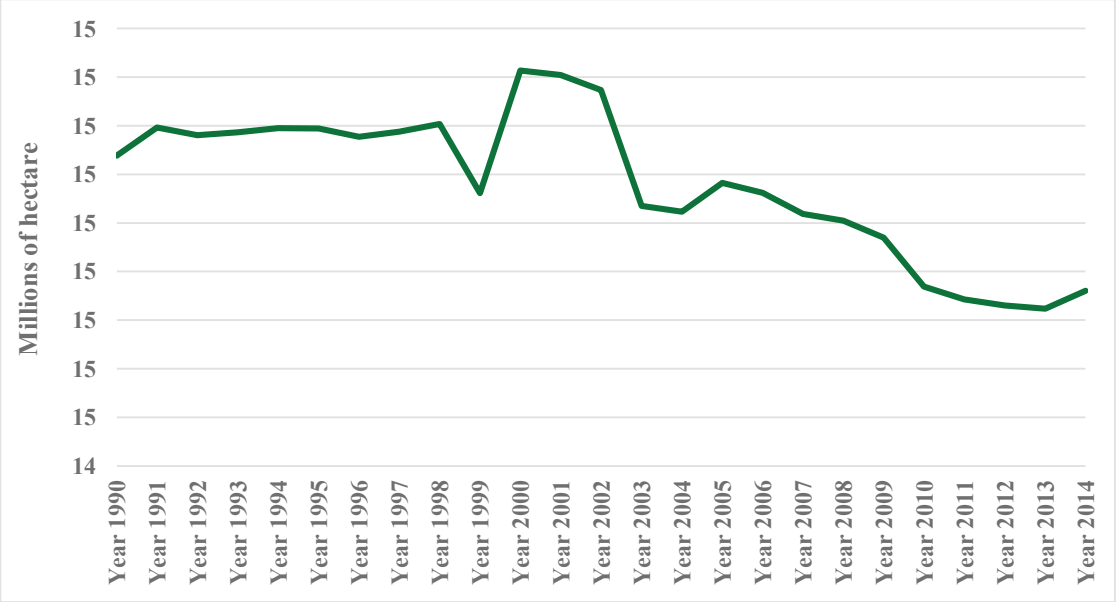

Figure 5. Land dedicated to agriculture in Romania (Land Matrix Global Observatory, 2017)

Figure 5 illustrate times series statistics collected by the National Institute of Statistics of Romania, showing that there was a decrease in the total surface dedicated to agriculture in Romania, except for the years 1999 to 2002. In fact, in 2013, this number was inferior to the 1990'.

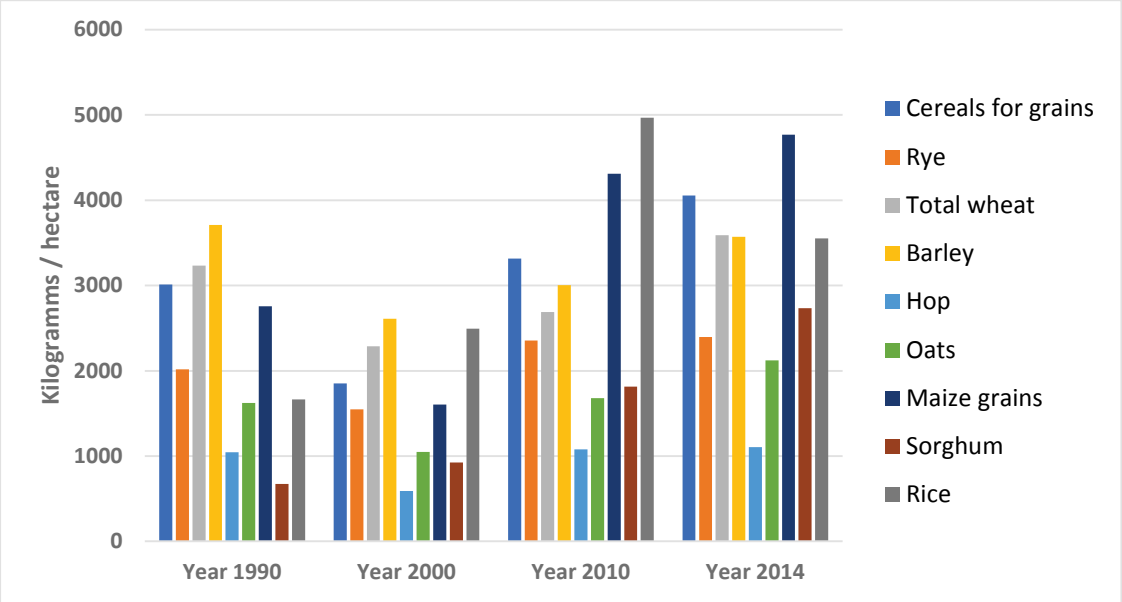

Figure 6. Average crop production per hectare in Romania (Land Matrix Global Observatory, 2017)

Figure 6 illustrates the average crop production per hectare and per year in Romania. Nine were selected amongst others. It is interesting to observe that the average crop production of some particular types of crops like maize grains, wheat and sorghum has widely increased between 1990 and 2014.

Finally, in **Table 1**, Land Matrix Global Observatory evidences of large land acquisitions by foreign investors in Romania are presented. What is important to remember is that land grabbing does imply large acquisitions by companies or foreign governments.

Investor country	Intention	Production size in hectare
Luxembourg	Food crops	6267
Denmark	Food crops	3000
Denmark	Food crops	2456
Italy	Food crops	10 500
Denmark	Agriunspecified	3105
United States of America	Food crops	9591

Lebanon	Agriunspecified	3192
Germany	Food crops	4165
Austria	Food crops	3798
Italy	Agriunspecified	4139
United Kingdom of Great Britain and Northern Ireland	Agriunspecified	5517

Table 1. Production size in hectare by land allocation and investor country in Romania (Land Matrix Global Observatory, 2017)

In short, there have been crucial changes in Romania these past few decades and studies that involved fieldwork have gathered this information. For example, according to Ecoruralis (2016), from 2002 to 2010, 150,000 small farms have disappeared while the number of large farms has increased by 3%. Currently, up to 10% of agricultural surfaces are in the hands of investors originating in third countries, and 20 to 30% of these are controlled by investors from the EU (EESC, 2015).

Actually, what is important to retain is that even if the total land dedicated to agriculture has decreased, it does not mean a lot for the average size of patches considered as crops. The average size of patches as well has the evolution of the landscape structure would instruct us about the type of agriculture, the disappearance of small-scale farming and the intention of these land allocation.

III. Methodology

Knowing that it is complicated to estimate land grabbing with studies involving fieldwork, remote sensing method with automatic process help to see the evolution of the sizes of the patches considered as crops over the years. The methodology was developed using image segmentation and the capacity of Google Earth Engine to identify object-based features in some of its large amount of freely available satellite images. The different parameters values were selected based on best-fitting visual results. The same parameters were implemented in the algorithm for the two different years even if different satellites were used. However, the Landsat band combination was carefully selected. Finally, it should be remembered that our intention is to assess land grabbing by looking at the evolution of sizes of patches considered as crops but not to give an exact number of this evolution.

This chapter will first review some fundamental concepts of remote sensing. Indeed, since spaceborne and airborne instruments were launched, consequent improvements were made and nowadays, a lot of different platform and data would be available to complete our task. It is also important to keep in mind the physics basics that are behind every remote sensing work because it allows us to understand the different properties of all data acquisition systems. Next, the data processing tool and the image-processing algorithm will be introduced; in other words, the different approaches followed to obtain the results. It is essential because the methodology that was selected influenced the results and the way they were interpreted.

1. Fundamental concepts of remote sensing

A. Physics basics

Electromagnetic radiation

First of all, as stated by Lillesand, Kiefer, & Chipman (2015), M is expressed by the Stefan Boltzmann law that states the higher the temperature of the radiator, the greater the total amount of radiation it emits. Therefore, that the energy is a function of temperature.

$$M = \sigma T^4 \quad \textbf{(1)}$$

M = total radiant exitance from the surface of a material [Watt m^{-2}]

σ = Stefan-Boltzmann constant [5.6697 x 10^{-8} E m^{-2} K^{-4}]

T = absolute temperature of the emitting material [K]

Then, the wavelength at which a blackbody radiation curve reaches a maximum is related to its temperature, by Wien's displacement law.

$$\lambda_m = \frac{A}{T} \tag{2}$$

λ_m = wavelength of maximum spectral radiant exitance [µm]
A = 2898 [µm K]
T = temperature [K]

Figure 7 illustrates the two implications of the equations above : both the quantity of energy that every object radiates and the spectral exitance are a function of the surface temperature of the object. Note that the sun temperature and the Earth ambient temperature are represented in yellow and in red respectively. It also means that for any wavelengths M is higher for the sun than for the objects on Earth. However, at is will be later explained, atmospheric perturbations will reduce M of the sun.

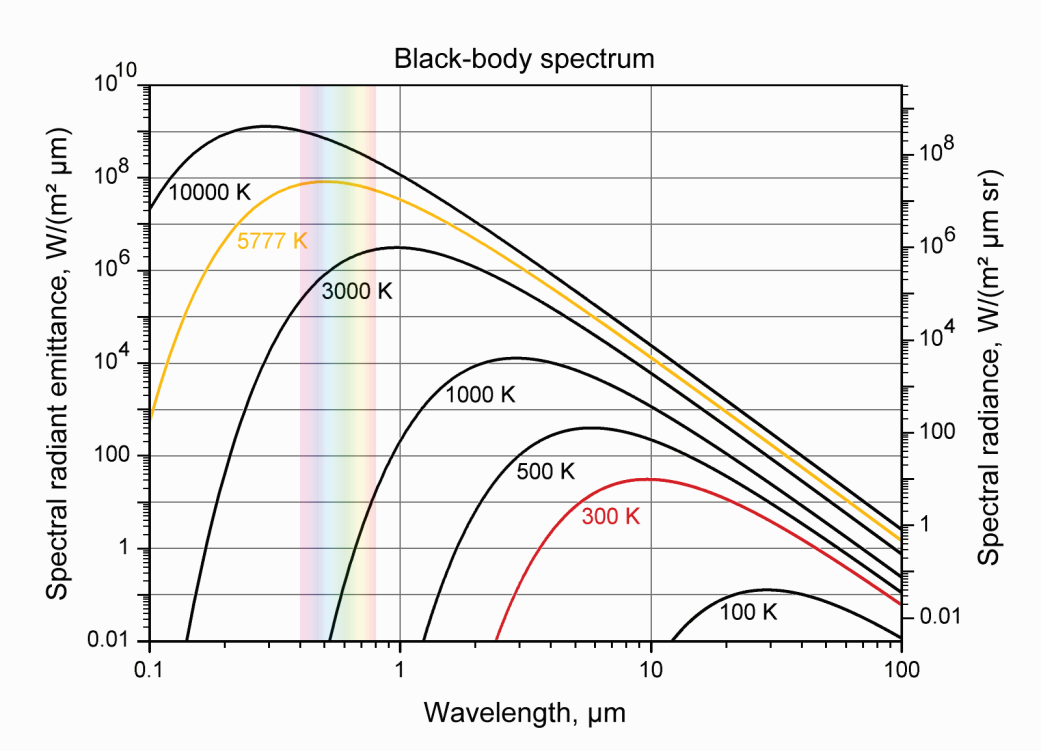

Figure 7. Black body Spectrum loglog (Sch, 2006). CC some rights reserved license

Electromagnetic radiation laws

The electromagnetic radiation laws concern all objects and matters with an absolute temperature above absolute zero. As explained above, M and λ_m values have important implications for remote sensing scanning systems. These values are ultimately linked to the basic wave theory more precisely, to how the radiation travels.

Electromagnetic energy is traveling in a harmonic, sinusoidal fashion at the velocity of light (c) (Campbell and Wynne, 2011). The distance from one peak to the next is the wavelength and the number of peaks passing a fixed point in space per unit time is the wave frequency v.

$$c = v\lambda \quad \textbf{(3)}$$

The equation above has several implications: the longer the wavelength, the lower the frequency will be. On the contrary, the shorter the wavelength, the higher the frequency will be.

From then on, Campbell and Wynne stated that (2011, p. 37) *"the wave model best explains some aspects of the observed behavior of electromagnetic energy (e.g., refraction by lenses and prisms and diffractions)".* Isaac Newton first recognized the dual nature of the light and later on, Planck and Einstein wrote modern theory explaining that the light is absorbed in discrete units (called photons). The size of this absorption is proportional to the frequency of the energy radiation, which has led to the Planck-Einstein relation or Planck's equation, which relates the energy of a photon to its frequency (Campbell and Wynne, 2011)

$$Q = hv \quad \textbf{(4)}$$

Q = Radiant energy [joule]
v = Frequency [Herz]
h = Planck's constant

Relating then this equation with $c = v\lambda$, low frequency and long wavelength will correspond to lower the radiant energy Q. This equation has again different implications when computing the radiant flux (Φ_e), the irradiance (E_e) or the radiant exitance (M_e).

$$\Phi e = \frac{\delta Q}{\delta t} \quad \textbf{(5)}$$

Φ_e = radiant flux [Watt s^{-1}] which is the energy delivered to a surface in a unit of time
Q = Radiant energy [joule]
t = time [seconds]

$$E_e = \frac{\delta \Phi e}{\delta A} \quad \textbf{(6)}$$

E_e = irradiance which is the rate at which radiation strikes a unit area [Watt/m^2]
Φe = Radiant flux received [Watt s^{-1}]
A = Area [square meter]

$$M_e = \frac{\delta \Phi e}{\delta A} \quad \textbf{(7)}$$

M_e = radiant exitance which is the rate at which radiation is emitted from a unit area [Watt/m^2]
Φe = Radiant flux emitted [Watt s^{-1}]
A =Area [square meter]

Figure 8 reviews the implications of the equations above. The frequency of electromagnetic radiations is linked to the fact that they travel at the speed of light (c) in harmonic, sinusoidal way. When frequency tend to increase, as c is a constant, λ tend to be shorter. Temperature of the body emitting at a given wavelength (K°) has implications for the radiant exitance as well as for the frequency, as described above.

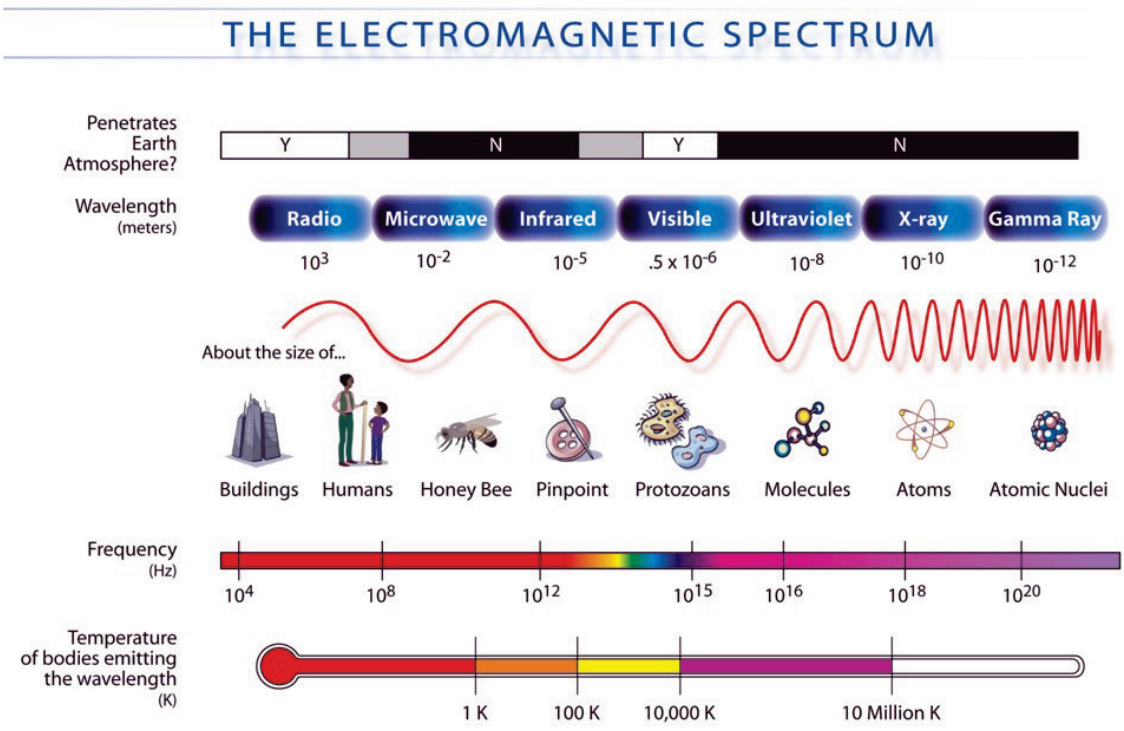

Figure 8. Electromagnetic spectrum (NASA, 2017). Public domain license

Human eyes and photographic sensors are sensitive to electromagnetic radiation of particular wavelength and magnitude when remote sensing scanning systems are receptive to others (Lillesand, Kiefer, & Chipman, 2015). To sum up, these electromagnetic radiation laws are important to understand because, long radiations lead to lower amount of radiation emitted per unit area, which tend to be harder for sensors to detect; like thermal IR energy. On the contrary, shorter wavelength radiation lead to higher energy and therefore are easier to sense; like visible light.

Atmospheric perturbations of electromagnetic radiation

Electromagnetic radiation is the information that is gathered by remote sensing systems. As seen above, the amount of energy can vary. Atmospheric perturbations can affect the electromagnetic radiations as well and hence the amount of energy gathered by the platform. Indeed, all radiation detected by remote sensors passes throughout some distance of atmosphere and this distance can affect the radiation by several mechanisms: scattering, absorption and refraction (Lillesand, Kiefer, & Chipman, 2015).

First of all, electromagnetic radiations can be affected by refraction which is, according to Campell and Wynne (2011, p. 43)*"the bending of light rays at the contact area between two media that transmit light"*.

Then, electromagnetic radiations can interact with smaller molecules that are present in the atmosphere such as H_2O molecules, dust or pollens (Girard & Girard, 1999). This effect is known as scattering. Two sorts of scattering can occur in the atmosphere: Mie scattering or Raleigh scattering, depending on λ, d (diameters of the molecules). Mie scattering occurs if $\lambda * 10^{-2} < d < \lambda * 10^{2}$ and is particularly important near industrial sites (Girard & Girard, 1999). The effect of Rayleigh scattering ($\lambda > d$) is inversely proportional to the fourth of power of wavelength, there is a much stronger tendency for short wavelengths to be scattered by this mechanism than long wavelength (Lillesand, Kiefer, & Chipman, 2015). Thus, shorter wavelengths (blue) are more dominantly scattered than longer ones and this is the reason why the sky appears to be blue, otherwise it would be black (Girard & Girard, 1999).

Finally, another effect on electromagnetic radiations is atmospheric absorption, which results in loss in energy at a given wavelength but the energy is nevertheless reradiated at longer wavelengths (Campbell & Wynne, 2011). Absorbers like water vapor, carbon dioxide and ozone are the most efficient absorbers but at specific wavelength (Lillesand, Kiefer, & Chipman, 2015). Due to that, in some spectral regions, the energy is blocked and therefore, the spectral sensitivity of the scanner must be carefully chosen.

Table 2 sums up the different absorption of electromagnetic radiation by water vapor, carbon dioxide and ozone. **Figure 9** illustrates the different atmospheric windows. The areas represented in blue are regions where the atmosphere is highly transmissible as the areas in white are regions where molecules absorb electromagnetic radiations and block the energy.

H_20	Lower atmosphere	from 5.5 to 7.0 µm above 27 µm
$C0_2$	Lower atmosphere	13 to 17.5 µm
0_3	Lower atmosphere	0.24 µm

Table 2. Atmospheric absorption by molecules. Adapted from Lillesand, Kiefer & Chipman (2015)

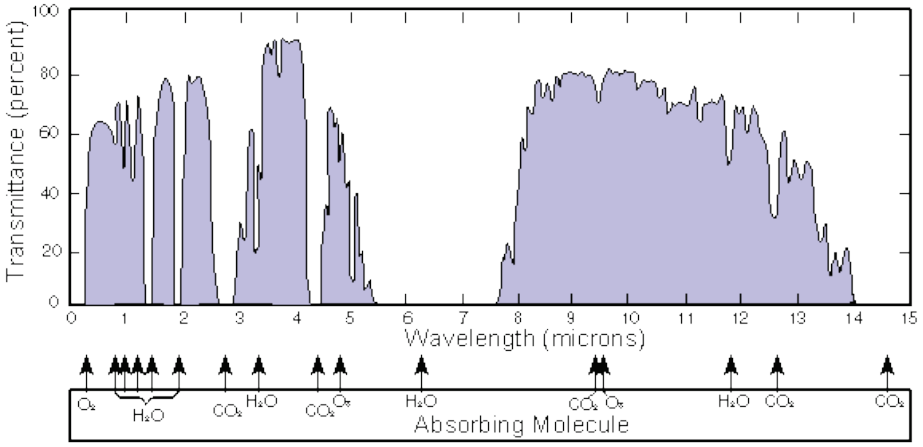

Figure 9. Atmospheric windows (U.S Navy, 2006). Public domain license

Surfaces interactions with electromagnetic radiations

Surface interactions with electromagnetic radiations are doubtless the most important property to understand in this chapter treating about remote sensing physics. This is because sensors gather information reflected by features such as soil, water or vegetation and it is this information that will be later treated as support for remote sensing studies. Following Campbell and Wynne (2011), four different interactions between the surface and the electromagnetic radiation exist:

- Reflection is the redirection of an electromagnetic radiation as it hits a surface. It varies depending on the surface irregularities

- Transmission which is the transition of a radiation through a surface without significant attenuation

- Fluorescence which is defined as the emission of a radiation from an object but in a different radiation wavelength that was received

- Reflectance which is the relative intensity of the radiation of a surface as measured for a specific wavelength interval

Reflectance is a property that should be detailed in a more precise way. As it was explained above, for each specific wavelength interval, there is a percentage of the incident electromagnetic radiation that is reflected. Moreover, sensors observe through different ranges. For example, multispectral sensors range from the visible to the thermal spectral region as thermal sensors observe in smaller range window (Lillesand, Kiefer, & Chipman, 2015).

Knowing that the proportions of energy reflected, absorbed and transmitted will vary for different earth features (depending on their material type and conditions) and depending on the wavelength, looking at the reflectance curve of a particular feature will help the user to choose the correct wavelength region for this particular research application (Lillesand, Kiefer, & Chipman, 2015). This characteristic can be expressed by the spectral reflectance, mathematically defined as:

$$\rho_\lambda = \frac{E_R(\lambda)}{E_I(\lambda)} = \frac{\text{(energy of wavelength } \lambda \text{ reflected)}}{\text{(energy of wavelenth } \lambda \text{ incident upon the object)}} * 100 \qquad \textbf{(8)}$$

Figure 10 shows the average reflectance curves for different features such as vegetation or water. A user that would like to discriminate soil properties will tend to look at the IR range and to choose the correct sensor. In the case of this work, as it is intended to have a careful look at vegetation, NIR range will be considered as well as using a remote sensing platform with the correct spectral band. Not to forget is the fact that different types of vegetation have different curves as well.

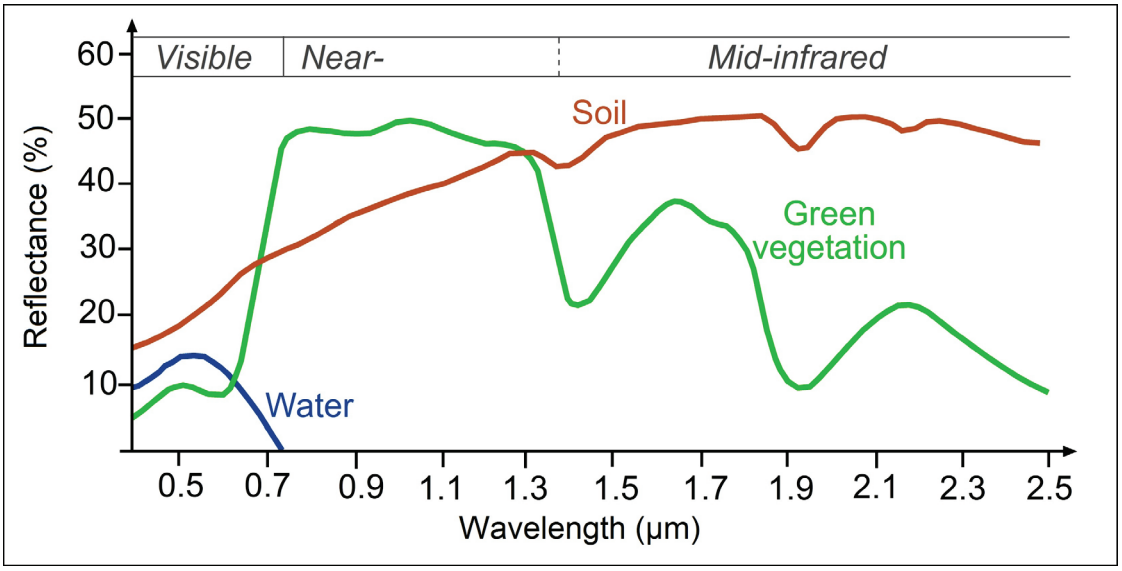

Figure 10. Average reflectance curves for different features (SEOS Project , 2017). CC some rights reserved license

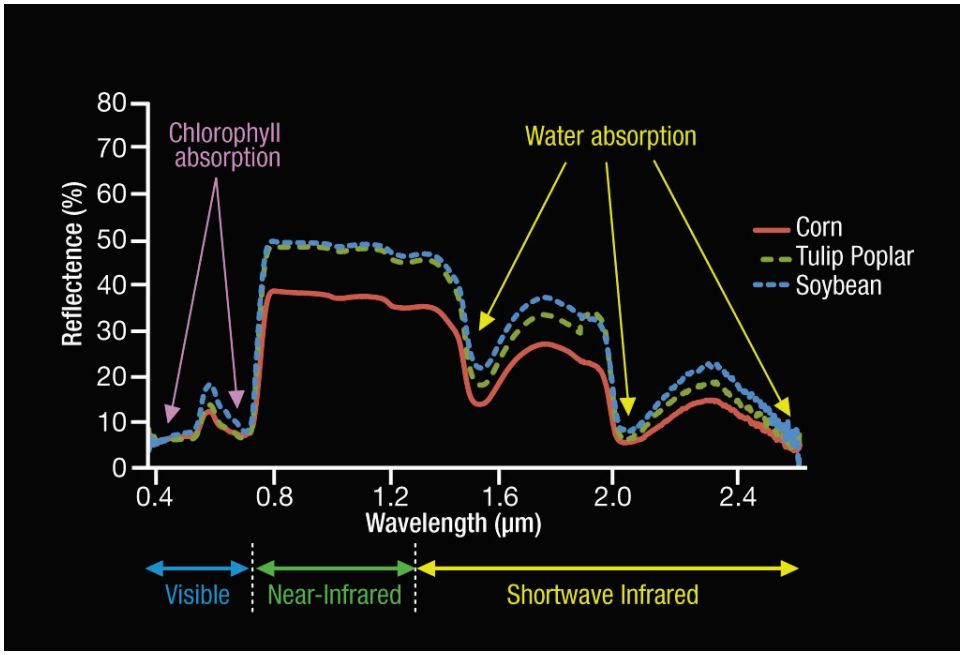

Figure 11. Spectral signature of different types of vegetation (Colstoun, 2010). Public domain license

Nevertheless, as stated by Lillesand and al. (2008, p. 22), *"spectral response patterns measured by remote sensors may be quantitative but they are not absolute, they may be distinctive but they are not necessarily unique"*. There are several reasons for this and it is important to keep this variability in mind for every particular remote sensing application. First, temporal, spatial or shadow effects can influence spectral response of the feature (Lillesand and al., 2008). As an example, temporal effect may be important to consider for the particular case of vegetation because of the growing cycle that goes through the year. Finally, atmospheric and geometric influence may be responsible of differences between spectral signature of the feature and the information recorded by the sensor (Lillesand and al., 2008).

B. Mapping systems

Earth observation tools also known as mapping systems are important to understand. Each instrument has different properties and this is why the platform and data that are chosen for a given study must be carefully selected. First, a distinction between the sensors available has to be done. Secondly, the difference between analog and digital data has to be explained. Finally, scanner differences will be explained.

Each instrument, like a satellite, is composed of a sensor but there are active and passive sensors. As stated by Campbell and Wynne (2011, p. 55), *"active sensors are active in the sense that they provide their own energy, so they are independent of solar and terrestrial radiation"*. Active instruments such as LiDAR or synthetic aperture radar for example can gather data whatever the weather conditions or the time of the day.

In the other hand, passive sensors acquire the energy that the objects are sending and according to Campbell and Wynne (2011, p. 54), *"this form of remote sensing mainly uses energy in the visible and near infrared portions of the spectrum"*.

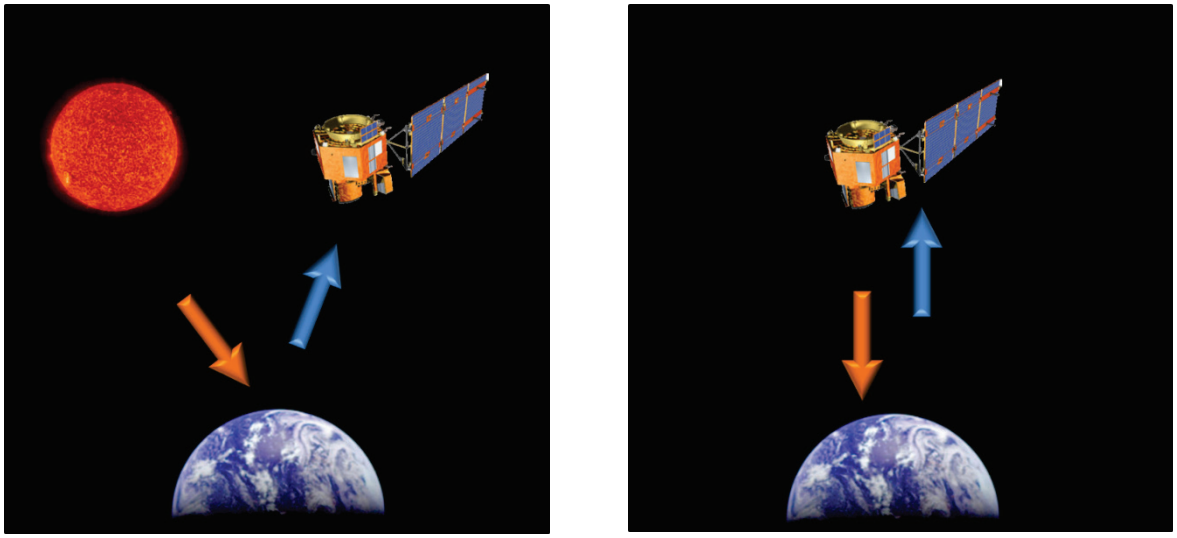

Figure 12. Passive sensor on the left and active sensor on the right (NASA, 2012). Public domain license

Land observation satellites images were used in this work but other remote sensing instruments exist and were used for decades before bringing to everyone's reach satellites images. Once, images were recorded on a physical form (analog data) made of paper or film with *"chemical coatings that record the patterns of the images"* (Campbell and Wynne, 2011, p. 101). For example, aerial photographs using passive sensors store analog data. They are still used but with disadvantages compared to digital data: the storage, the transmission and analysis difficulties (Campbell & Wynne, 2011).

Most of the images are nowadays recorded in a digital way. Sensors are loaded on platforms and they systematically scan portions of the Earth surface recording photons emitted from individual patches of ground that are known as pixels and giving each pixel a numeric value according to the region they belong on the electromagnetic spectrum (Campbell & Wynne, 2011). As stated in the previous sections, spectral responses of feature on earth surface are different: soil, sand, vegetation, snow or water for example. In an 8 bits system, digital values would range from 0 to 255 (depending on their spectral response) and can then be easily interpreted with the help of a computer (Campbell & Wynne, 2011). Indeed, images are composed of arrays each containing pixels, which individually could not be interpreted by the human eye.

65	74	81	121	128	157	177	182	208	205	205	215	226	232	235	238	246	251
55	64	73	72	57	88	110	111	153	188	202	216	223	218	220	231	242	244
65	61	62	67	75	71	70	73	87	129	149	169	190	204	214	222	227	223
73	70	65	72	70	67	70	64	57	72	67	89	127	166	193	206	216	221
66	72	76	75	78	65	71	73	57	60	63	74	77	89	128	167	193	205
91	103	99	101	85	88	85	76	73	72	66	65	71	70	72	83	110	141
109	117	125	114	105	104	94	93	85	94	76	65	62	66	78	72	56	77
104	117	139	123	126	120	111	111	100	110	99	83	88	76	62	66	64	79
111	124	138	137	136	138	133	120	121	114	92	90	91	75	80	84	63	68
113	125	135	137	139	137	138	134	129	127	144	123	123	108	96	93	77	68
95	113	129	129	139	144	143	155	136	146	148	134	123	117	112	101	81	79
88	97	106	127	126	159	156	163	141	145	144	134	129	128	114	98	89	83
69	84	97	105	120	142	150	154	147	146	145	138	129	122	106	96	90	80
64	78	89	96	105	123	135	138	141	141	149	131	119	114	102	90	77	71
47	62	72	88	96	108	112	112	126	132	124	121	109	97	103	89	62	68
36	53	65	75	78	90	103	100	114	107	101	93	98	84	72	72	56	47
24	39	52	64	66	78	90	83	93	85	80	77	76	56	52	57	42	46
21	29	36	51	60	65	67	61	71	72	69	50	56	54	42	45	47	42
26	32	33	34	36	44	51	55	54	50	51	50	46	45	44	36	31	39
11	19	25	25	28	38	40	48	41	42	37	49	47	40	39	37	40	49
37	38	28	34	44	43	34	35	41	39	40	48	49	44	42	41	42	45
94	96	114	115	110	103	100	95	89	84	72	63	55	51	49	47	48	50
172	173	171	175	172	172	179	173	156	150	140	122	113	107	99	88	84	81
195	192	190	193	193	192	198	197	194	194	191	180	180	180	168	157	156	152
227	230	226	225	228	225	216	215	217	214	208	203	205	203	194	190	195	189

Figure 13. Pixels array of puzzle image displayed in Matlab

Moreover, digital data contained in the images are recorded by different types of scanner: multispectral, thermal, hyperspectral or optical mechanical scanner which are different in their design (De Morsier, 2016). Actually, each of these different scanners have a particular photometric system. Photometric systems are sets of different spectral bands. Spectral bands record portions of the electromagnetic spectrum but each of them through a different window.

As an example, Landsat 5 multispectral scanner include four bands (U.S. Geological Survey, 2017) :

- band 1: 0.5-0.6 µm
- band 2: 0.6-0.7 µm
- band 3: 0.7-0.8 µm
- band 4: 0.8-1.1 µm

Finally, systems, like satellites, have different abilities to record details and in other words their resolution is different. Additionally, as stated by the NASA there are different types of resolution and usually a trade-off between these different resolutions is needed (NASA, 1999) :

- Spatial resolution: area of a single data point on Earth's surface, in other words the optical quality of an image. For example: 30 meters or 250 meters
- Spectral resolution: number of wavelengths of the electromagnetic spectrum in which a given satellite sensor "sees" the Earth. For example, MODIS satellite records images at 36 different spectral wavelengths as others like MISR only at four different ones.
- Temporal resolution: intervals at which sequences are recorded. For example: 1-2 days or 5 years

2. Data processing tool

In order to reveal what is unnoticeable with a visual exploration, different processing steps needs to be achieved. Long-term change detection and large-scale processing are wanted to achieve this work. Software's like MATLAB or ERDAS IMAGINE provide processing tools that do not require considerable technical skills but the data can only be downloaded and processed scene by scene. Bad quality image and long downloading process can easily happen. On the contrary, considerable technical expertise and effort are required to use tools (TerraLib, Hadoop, GeoSpark and GeoMesa), designed to facilitate large-scale processing (Gorelick, et al., 2017).

Given these two elements, GOOGLE EARTH ENGINE has been used for this work. It provides a cloud platform to access and process large amount of freely available satellites images. Simple analyses with the explorer interface can be performed as well as complex geospatial workflow using the code editor, in order to reveal what is unnoticeable with a visual exploration. Huge dataset, API tutorial, online sharing and friendly interface can be listed as the main advantage of this platform. As an example, **Figure 14** is part of an algorithm available on the GEE platform.

It is an edge detection algorithm that is applicable to a specific area or the whole world. There are several specialized edge detection algorithms available. The Canny edge detection algorithm was used to detect edges in **Figure 15** and the result is displayed in **Figure 16**. The algorithm does the following things (Google Developers , 2017) :

- It uses four separate filters to identify the diagonal, vertical, and horizontal edges
- The calculation extracts the first derivative value for the horizontal and vertical directions and computes the gradient magnitude
- Gradients of smaller magnitude are suppressed

```
// Load a Landsat 8 image, select the panchromatic band.
var image = ee.Image('LANDSAT/LC8_L1T/LC80440342014077LGN00').select('B8');

// Perform Canny edge detection and display the result.
var canny = ee.Algorithms.CannyEdgeDetector({
  image: image, threshold: 10, sigma: 1
});
Map.setCenter(-122.054, 37.7295, 10);
Map.addLayer(canny, {}, 'canny');
```

Figure 14. Canny edge detection algorithm. Google Earth Engine API (2016).

Figure 15. Satellite imagery of the region of Lausanne 2017

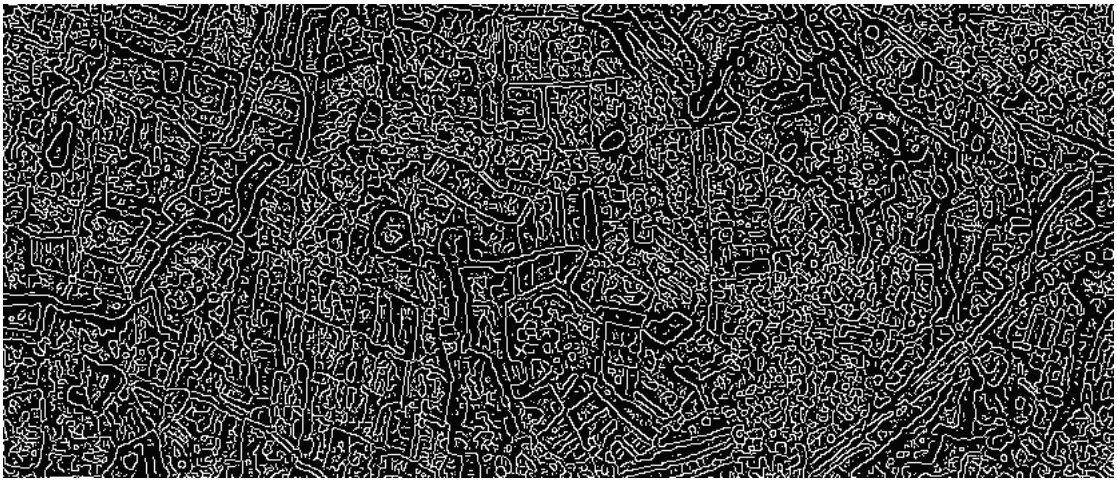

Figure 16. Canny edge detection algorithm of figure 15

3. Image processing algorithm

Different satellites imagery from different satellites were used for this work. First of all, we wish to improve the images to suppress unwilling distortions as well as enhance the image features that are important to detect patches of crops (Boyle, Sonka, & Hlavac, 1993). One means to cope with this situation is to carefully choose the image and then to apply some basic preprocessing tools on the image.

For that matter, the different images should have been taken in the same season, in order to minimize the difference due to the phenological changes. In this work, we are interested in dealing with changes in vegetation and size of patches of crops. As crops have their high growing season in summer, only images from this particular time of the year have been used (1st July to 1st September).

Then, clouds should be removed from the area of analysis by creating a cloud-free image composite with custom parameters. Google Earth Engine provides the Landsat.simpleComposite algorithm. To remove the clouds it *"computes a Landsat TOA composite from a collection of raw Landsat scenes and it applies standard TOA calibration and then assigns a cloud score to each pixel using the SimpleLandsatCloudScore algorithm"* (Google Developers, 2017). This algorithm selects the lowest possible range of cloud scores at each point and then computes per-band percentile values from the accepted pixels.

Moreover, to avoid the platform to be solicited when not compulsory, only the area of interest should be saved. The solution that was kept was to filter the images by bounds, in other words, by the computation were only made on particular counties of Romania. The images were also filtered by land use in order to only keep the part of land we are interested in. This means that a land use raster dataset was implemented and that computation were only made on the agricultural part of the land.

Finally, the Normalized Difference Vegetation Index (NDVI) was computed and used as original image for this work. This is because and as stated by Soille (2000, p. 1025), *"vegetation has a significantly higher reflectance than soil for wavelengths around 800 nm under natural daylight (direct or diffuse)*. This index is based on the difference of reflectance in the near-infrared and red bands: $\frac{\rho\ NIR - \rho\ RED}{\rho\ NIR + \rho\ RED}$; vegetation will have higher NDVI values than non-vegetated areas and they will be therefore more easily differentiable (Lillesand, Kiefer, & Chipman, 2015).

A. Image segmentation using edge detection

Raw images are unlikely to perform and quantify the changes between two periods. One means of dealing with this is to perform image segmentation using edge detection. As stated by Campbell and Wynne (2011, p. 371), segmentation is "*the identification of the edges of homogeneous patches that subdivide the image into interlocking regions"*. In other words, simplify the representation of the image into something that is more meaningful and where it is easier to extract information: make single pixels to become objects. As *"spectral characteristics are not always fully evaluated in visual interpretation"* and spectral patterns are highly informative, digital image data are preferably analyzed (Lillesand, Kiefer, & Chipman, 2015).

To sum up, this process labels pixels into groups of spatially connected pixels. These groups or patches share the same spectral characteristics like the intensity of each pixels, which corresponds to their average radiance. It is characterized by a digital number (DNs), which is a positive integer value and there is a DNs for each pixel (Lillesand, Kiefer, & Chipman, 2015). Statistics or size and shape analysis based on these patches can be performed (De Morsier, 2016).

Low-pass filtering

Starting a segmentation without having previously filtered the image would certainly lead to a noisy result, meaning that there would be too many details in our segmentation. This is because perturbations caused by artefacts due to the process of acquisition are common in images (Girard & Girard, 1999). Smoothing the image using a filter in order to remove isolated local details that would interfere with the global structure is therefore wanted. In other words, image smoothing is commonly used to improve visual appearance and simplify image segmentation by reducing the noise and preserving important features such as homogenous regions, discontinuities, edges and textures (Grazzini & Soille, 2009).

For that matter, as stated by Serra (1988), any filtering operation made on the image G can be expressed as the dot product $F * B$ or convolution operation. B being a 2D moving window, in other words, the pixels considered by the convolution. The convolution filter F, also called kernel, has the same size as the moving window.

Different categories of filters exist, low and high-pass filter amongst others. Other types of low-pass filters exist such as mean or Gaussian filter but median was chosen because *"it preserves edges whilst removing noise*" (Angalaparameswari & Senthilkumar, 2014, p. 30). The median kernel was created with the given parameters:

Radius	4

The convolution operation was applied on the NDVI images using the median kernel. It results in a smoothed image that has been removed of isolated local details that would interfere with the global structure.

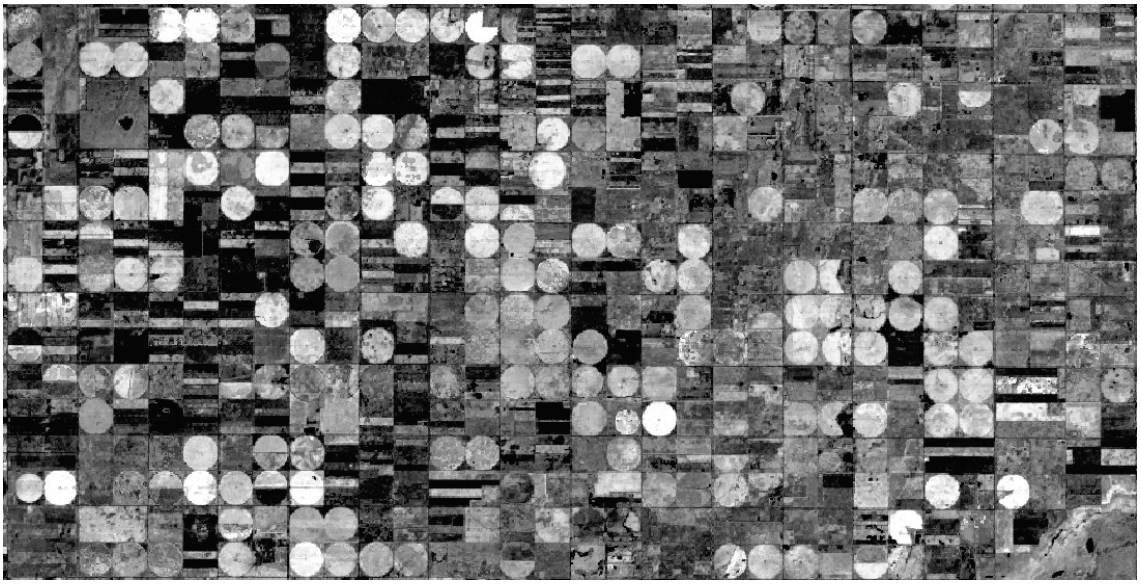

Figure 17. Prior to convolution

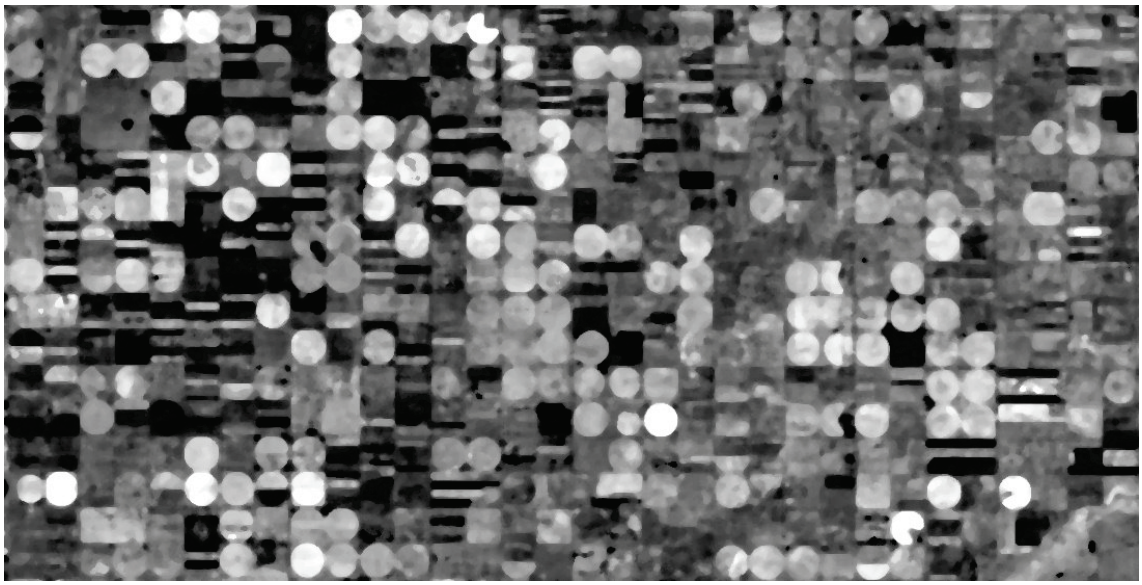

Figure 18. After the convolution

Image segmentation

Image segmentation can be performed by various methods like clustering methods, edge-based methods or region-based methods and each method relies on different information to perform the segmentation: for example, clustering methods rely on spectral information as edge-based methods rely on pixels (De Morsier, 2016). For this work, an edge-based method has been chosen principally because this method labels pixels within the same edge boundaries.

Moreover, edge-based methods can be performed by various algorithms. Some are based on first order derivative approaches like canny edge algorithm as others are based on second order derivative approaches like zero crossing algorithm. First order edge detectors measure the intensity gradient at a point in the image as second order detector try to find the peaks in gradient magnitude directly (Morse, 2000). These methods are built on the assumption that outline of objects are areas where there are strong variations of grey-level and that these regions can be outlined by studying the derivative of the image function (Girard & Girard, 1999).

For this work, zero crossing algorithm was chosen because *"this offers the possibility to determine edge positions to the accuracy of one pixel by using second derivative filters"* (Canty, 2010, p. 142).Mathematically, various operations are happening in order to build the algorithm that will filter the image. Following Canty (2010), the different steps that lead to a segmented image using the zero-crossing algorithm are explained below.

1) Image is composed of digital numbers and each pixel needs to be filtered on by one

x1	x2	x3	x4	x5
x6	x7	x8	x9	x10
x11	x12	x13	x14	x15
x16	x17	x18	x19	x20
x21	x22	x23	x24	x25

2) For each pixel of the image, the Laplacian operator ∇^2, the second derivatives of the image intensities are computed. It is defined by:

$$\nabla^2 = \frac{\partial^2}{\partial x^2} I(x,y) + \frac{\partial^2}{\partial y^2} I(x,y) \quad \textbf{(9)}$$

3) As an image is represented with discrete pixels, the Laplacian has to be approximated by a discrete convolution kernel. For this work, the kernel was chosen on a visual basis. This means that a lot of different kernel were tested until the best one was found. The negative value in the center is there to enhance the edges.

$$h = \begin{pmatrix} 8 & 8 & 8 \\ 8 & -63 & 8 \\ 8 & 8 & 8 \end{pmatrix}$$

4) Then, a convolution is performed between the Laplacian kernel created above and the image that was convolved previously. This is because, as stated above by Serra (1988), any filtering operation made on the image G can be expressed as the dot product $F * B$or convolution operation. B being a 2D moving window, in other words, the pixels considered by the convolution. The convolution filter F, or kernel, has the same size as the moving window.

5) Finally, it is by studying the image function that the algorithm, will detect edges. They are the places where the length of the Laplacian vector estimate$[u, v] = (\nabla I)$exceeds some threshold value: zones of strong variation. Indeed, the Laplacian is an isotropic scalar function which is zero whenever the gradient magnitude is maximum (constant intensity) and has opposite signs immediately on either side (change in intensity).

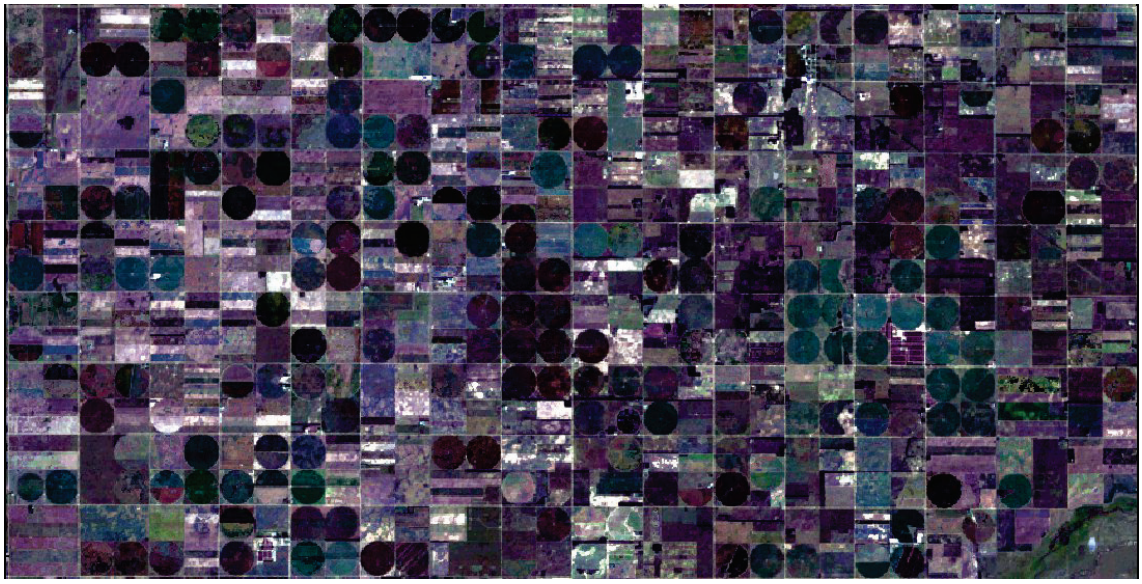

Figure 19. Original cloud free image

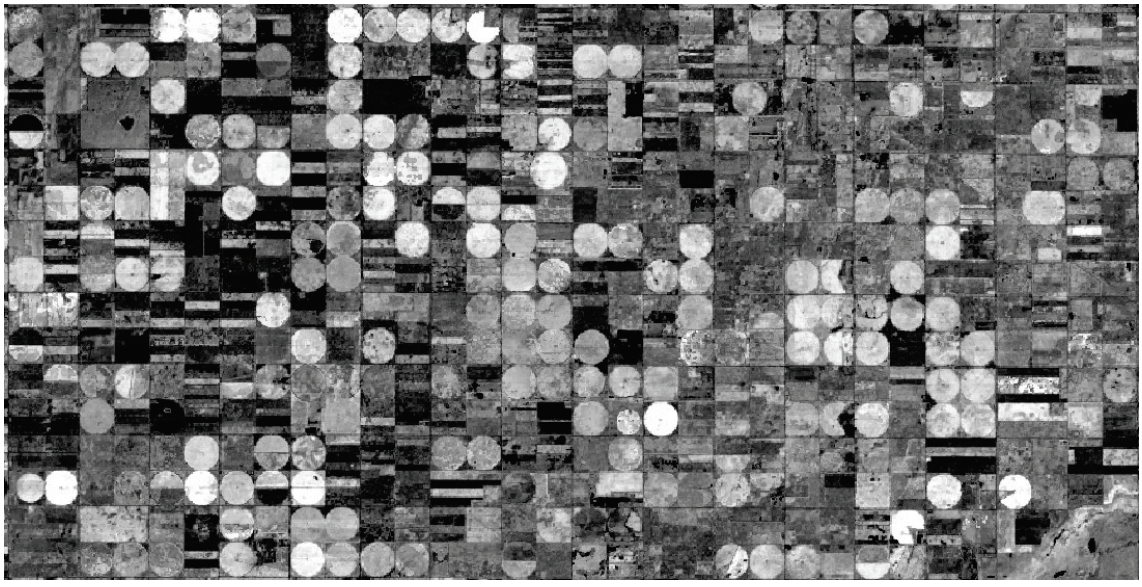

Figure 20. NDVI cloud free image.

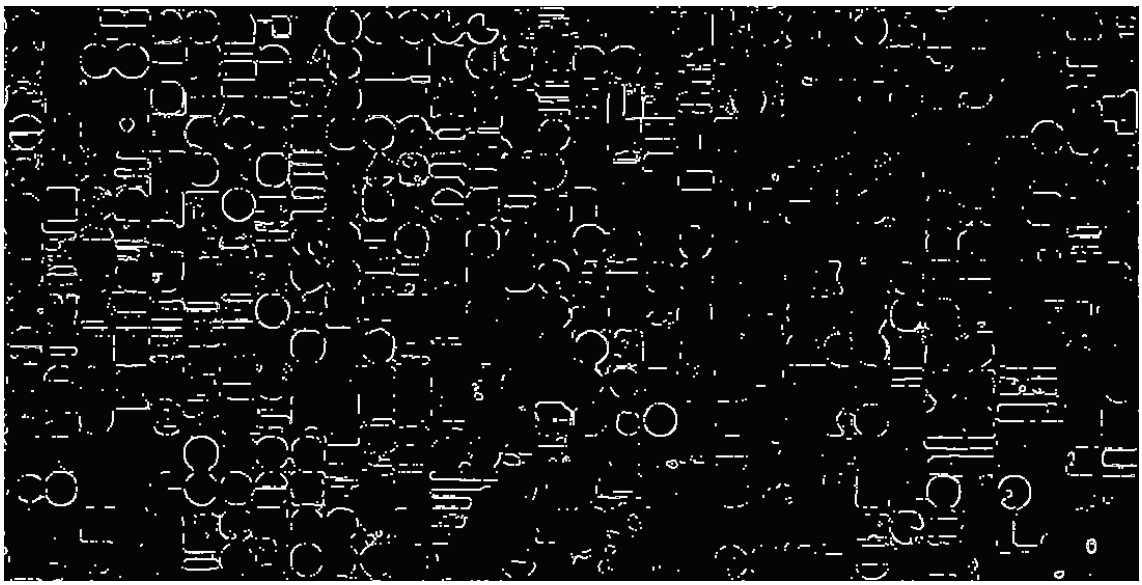

Figure 21. Over segmented region.

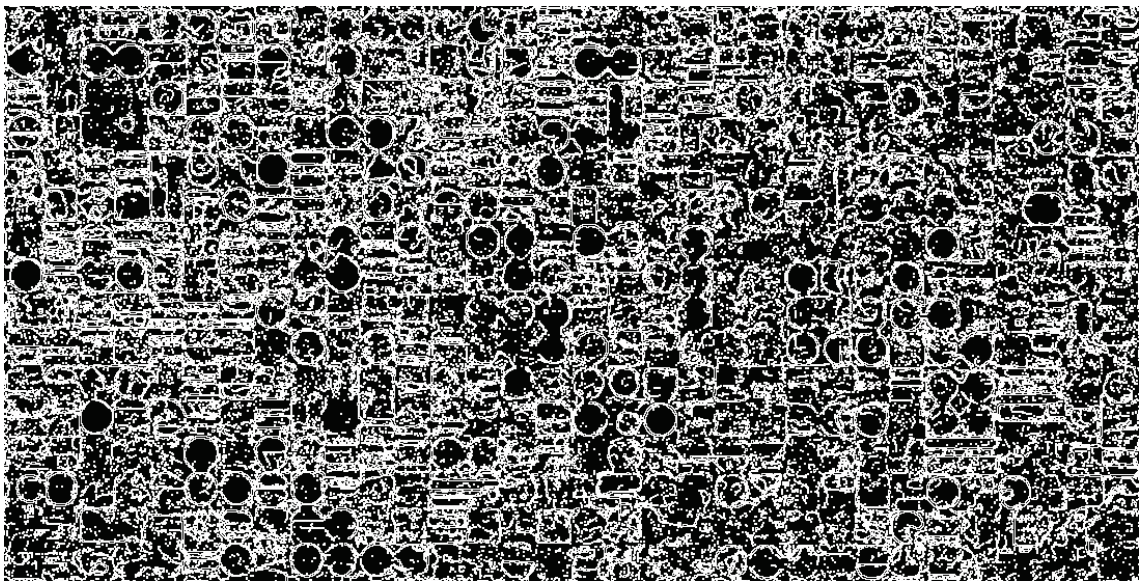

Figure 22. Under segmented region

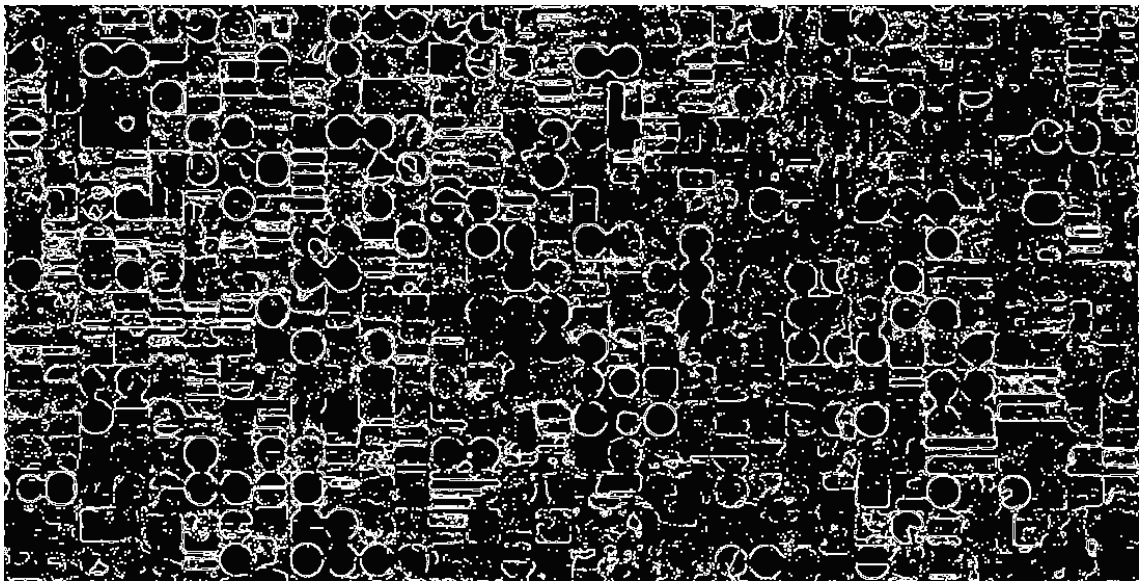

Figure 23. Correctly segmented region.

Binary image

To sum up, the algorithm automatically thresholds the image into two classes so additional processing can be applied to each class independently. In other words, a binary image has been produced where each pixel has been assigned a given value: 0 or 1 (Soille, 2000).

Figure 24. Original image (Sweeney, 2009)

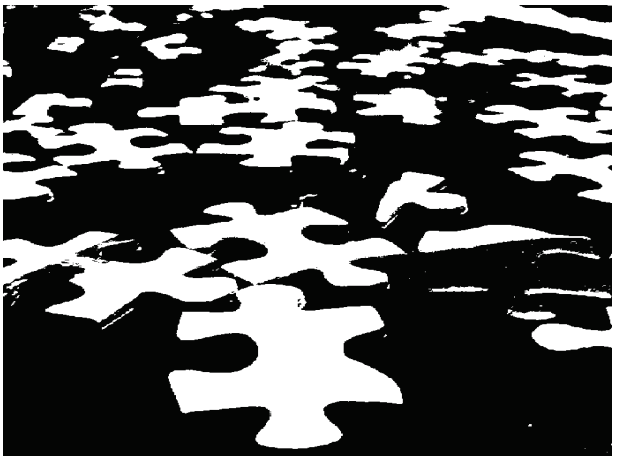

Figure 25. Binary image

B. Morphological operation

The images that were structured by the segmentation algorithm have yet no recognizable patterns: not all patches are "closed". This fact leads to a difficult interpretation in terms of size and shape analysis. One means of dealing with this problem is to perform a morphological operation on the desired objects, in our case, the "lines" that represents the edges of the patches. In other words, to apply morphological operations to the segmented image to close the edges.

Filter operations that were previously made, such as noise filter, rely on linear algebra but morphological operations rely on set theory: intersection, union or inclusion and different aspects have to be considered (Girard & Girard, 1999) :

1) Given a particular object and X the set of points that constitute this object
2) Given a structuring element B which shape is known: a circle for example
3) Check the subset relation between X and B by moving B in every point of space:
    a. If B falls inside (is totally included in X): $B \subset X$,
       it is an erosion: $(X \oplus B)$
    b. If B has at least on common point with A: $(B \cap X) \neq \emptyset$,
       it is a dilatation: $(X \ominus B)$
4) The points that satisfies either a. or b. make a new set of points called A

Combining these operations leads to interesting and contrasting results. Mathematically, morphological opening of given set X is the erosion of the dilatation of X: $X \circ B = (X \ominus B) \oplus B$ and morphological closing is the dilatation of the erosion of X: $X \circ B = (X \oplus B) \ominus B$.

Visually then, both of them provide distinct results as in **Figure 26,** opening removes small objects from the foreground of an image, placing them in the background, while in **Figure 27** closing removes small holes in the foreground, changing small islands of background into foreground (Pawar & Banga , 2012).

Figure 26. Closing

Figure 27. Opening

In the case of this work, a morphological closing has been performed because we wanted small gaps that were noticeable in the edges of the patches to be closed. More precisely, the parameters that were implemented were the following ones:

	Kernel 1: dilatation	**Kernel 2: erosion**
Radius	2	1
Iterations	1	1

The patches, which are delimited by edges but not entirely closed, are now correctly bounded and easier to label. Morphological operation has led to an image with much clearer bounds and patches are yet easily visually detectable

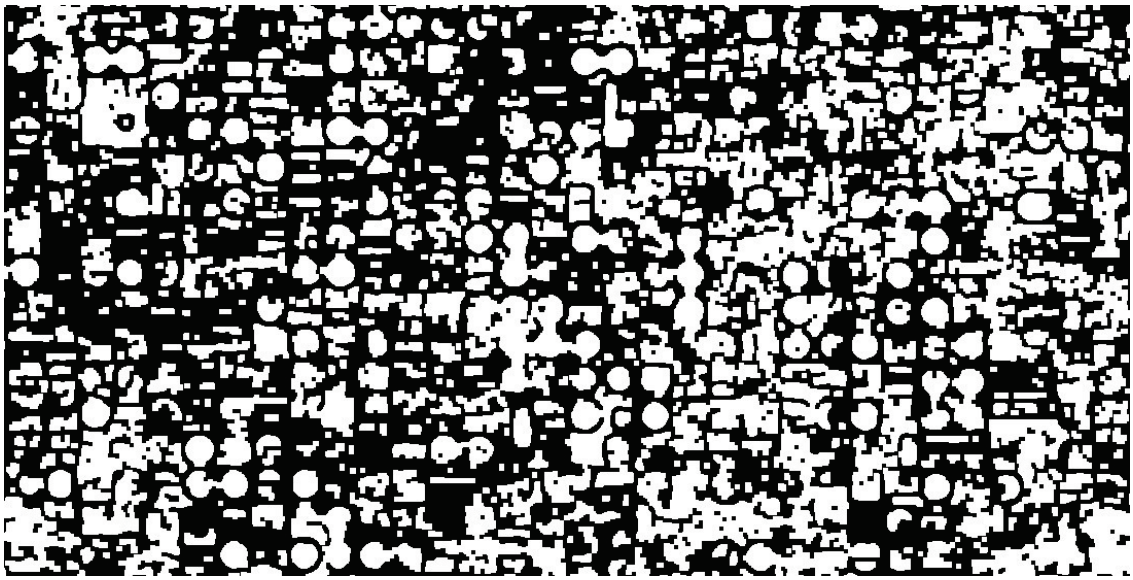

Figure 28. Morphological closing applied to segmented image.

C. Reducing patches into vectors and computing size

Starting from the binary image, pixels with values of zero were not considered. The binary image is a raster which can be defined as images such as scanned plans, aerial photographs, satellite images that are georeferenced (Ecole Nationale des Sciences Géographiques, 2013) . Then, the size of each of these patches is wanted. To do so, this raster is converted to vector which is a geometric object such as point, line or polygons that represent a geographic feature (Ecole Nationale des Sciences Géographiques, 2013), in our case, a patch considered to be a crop. The platform has an algorithm that is called reduceToVectors: it makes the process automatic. These vectors allow us to compute the areas of each vectors with a special function that was created and that computes the size of each vectors is square meters. A conversion into hectare was later made.

D. Workflow / Research design

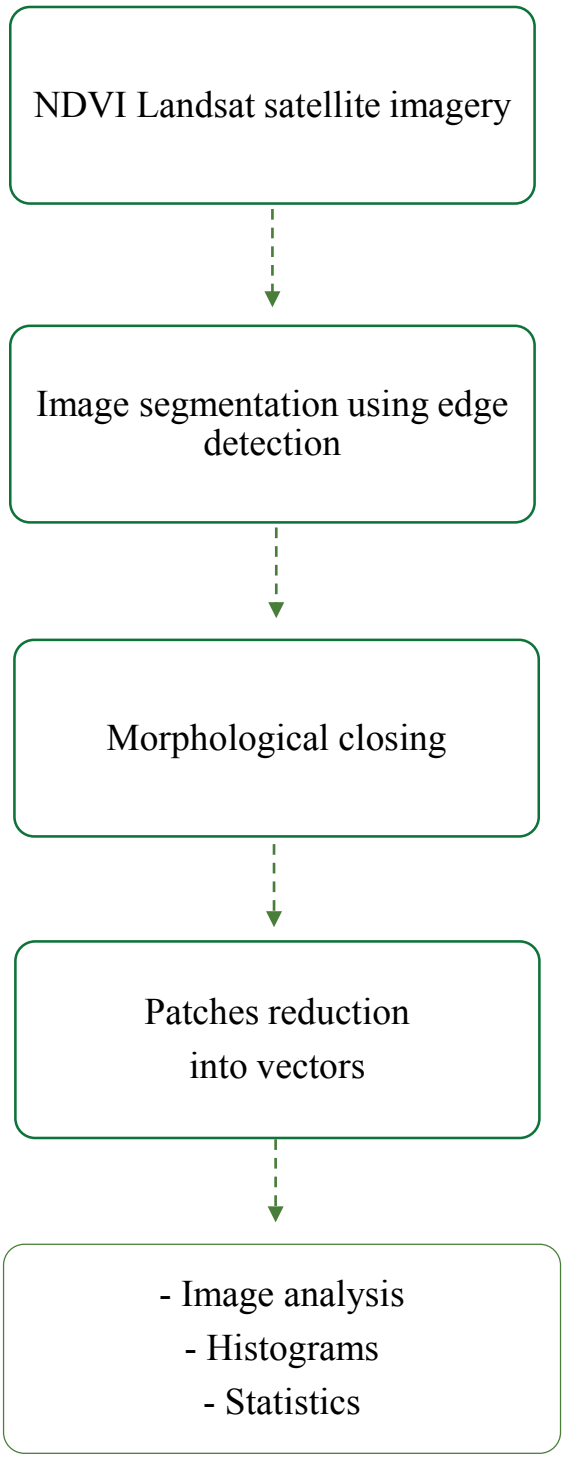

Figure 29. Workflow / Research design

IV. Case study

A. Study site

Given that it is not the entire country that is relevant for the question of land grabbing and that Google Earth Engine is not yet able to compute statistics for the whole country well enough, a selection among regions of Romania was made. There is actually 41 counties (Judet) in Romania, which corresponds to regional states. Four of them were chosen to perform the study on land grabbing: Ialomita, Călăraşi, Brăila and Buzău. These counties are located in the East of the country. They were selected based on two criteria:

- Suspicion of land grabbing reported by Land Matrix Global Observatory
- Agricultural subsidies in Romania reported by EcoRuralis foundation

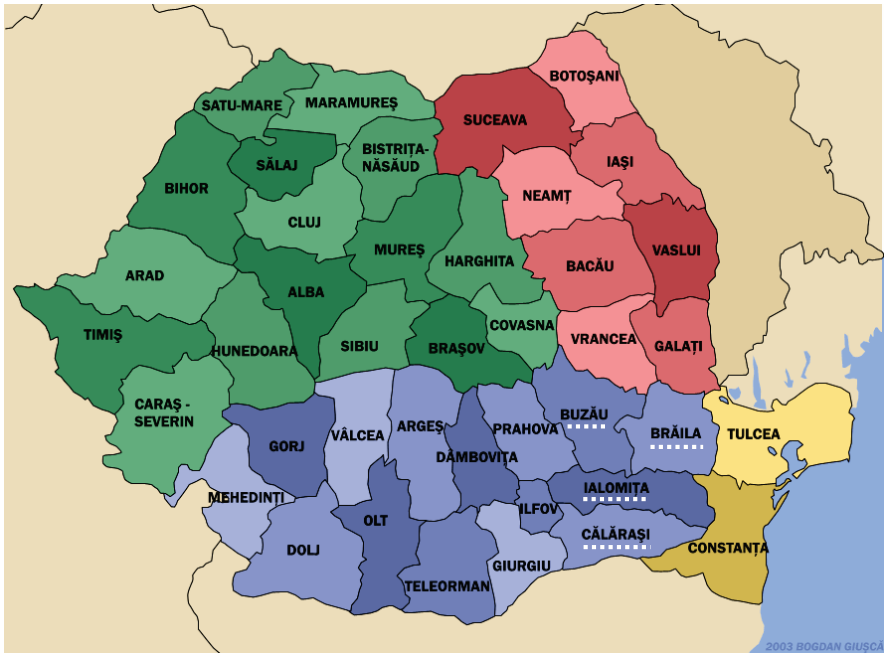

Figure 30. Counties of Romania (Giuşcà, 2005). CC some rights reserved license

B. Data

For the four areas of interests, imagery of three different time frames was selected, corresponding to mid-summer growing season periods: August 2006, 2011 and 2016. These specific years were selected because Romania joined the EU in 2006 and a change detection for a 10 year period was desired. Moreover, the month of August was carefully chosen because it represents the peak of crops growing season.

The images were taken from different Landsat satellite missions. The first mission was launched by the United States in 1972, in the time of the lunar missions such as Apollo. As stated by NASA (2017), *"It was the first Earth-observing satellite to be launched with the express intent to study and monitor our planet's landmasses"*. For our study, the visible (green and red) and near infrared (NIR) bands were selected, each with 30 m spatial resolution. Landsat 5 (1983-2013) Raw Scenes (Orthorectified) and Landsat 8 (2013) Raw Scenes (Orthorectified) images where selected in the Google Earth Engine catalogue.

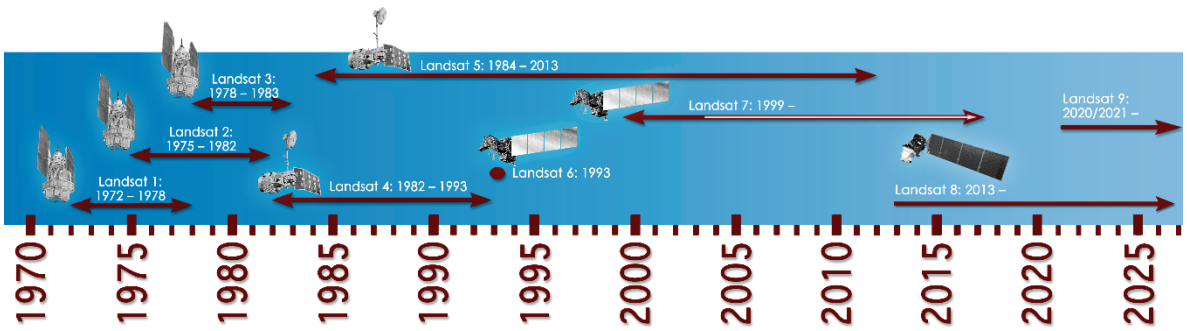

Figure 31. Landsat timeline (NASA, 2017). Public domain license

To complete our analysis, Corine (Coordination de l'information sur l'environnement) land cover raster was used as additional data. This program was created in 1985 and the data used as the main source of information for the photo-interpretation of the images is provided by SPOT and LANDSAT satellites and with the help of topographical maps, aerial photographs and field data.

This step was important because a differentiation between agricultural and non-agricultural area was needed. Indeed, Corine was used to delineate the agricultural areas because quantification of changes in non-agricultural areas was not wanted. Threshold value on the NDIV layer was not possible, as was not classification within the platform.

This land cover raster is composed of 44 different land cover classes. In this work, only the categories which concerned agriculture were selected (12-22). Furthermore, this program is completed approximately every six years but we worked only with the 2006 dataset because we hypothesize that the land use does not considerably change in 10 years.

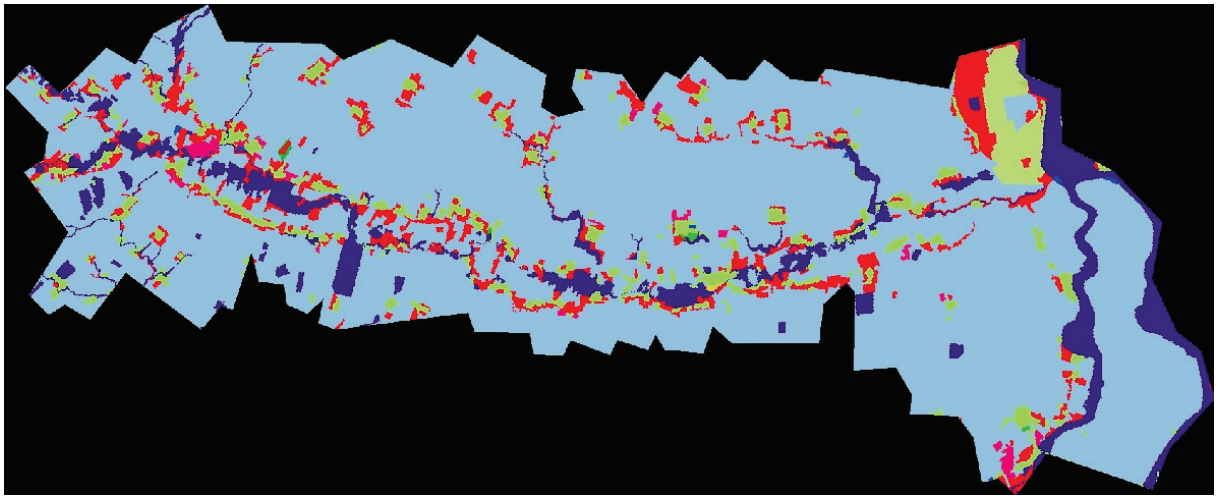

Figure 32. Corine land cover raster 2006. Ialomita County

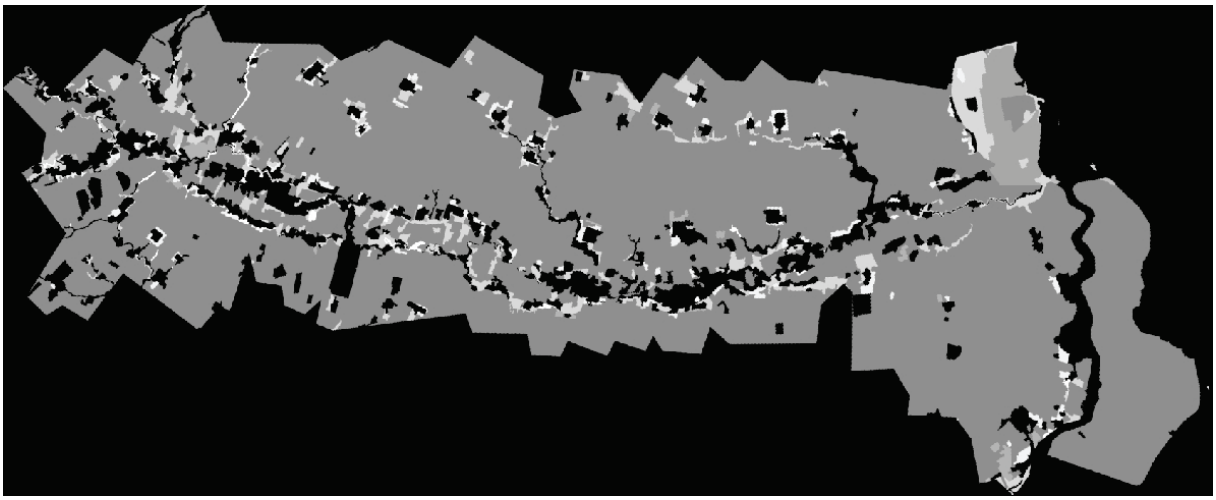

Figure 33. Corine land cover raster 2006 filtered by agricultural land use. Ialomita County

C. Results

In this chapter, we focus on the results of four counties in Romania at different time. Following the image-processing step, the data obtained were sorted out. Indeed, a large number of patches considered as crops were identified by the algorithm and extracted with the reduceToVectors algorithm and hectare computation function.

However, a threshold area value was implemented. Patches under the size of two hectares were not considered. Indeed, as stated by the European Union (2017), farms are considered to be physically very small when their agricultural area is less than two hectares. Patches that were too small to be considered as crops or noise were at the same time excluded. Patches above 500 hectares in size were also not considered. As a matter of fact, their number is yet too small to be considered as scientifically relevant and they are hard to detect with the segmentation. Indeed, very large patches may have been split into many when there were variations in surface features. We used the following categories :

- Small-sized patches considered as crops : 2 to 20 hectares
- Medium-sized patches considered as crops : 20 to 100 hectares
- Large-sized patches considered as crops : 100 to 500 hectares

Crops detection on Landsat images and resulting morphological operation

Here we compare Landsat images and the visual results obtained after performing the algorithm. These images are valuable because the parameters values for the algorithm were chosen on the best-fitting visual result. **Figures 33 to 40** are NDVI images of Landsat 5 (2006) and Landsat 8 (2016) and the result of the morphological operation performed on these images. It is displayed for the four counties we are interested in.

First, the NDVI images reveal recognizable features that are useful to make inferences about the environment. The images involve many patches of crops that are recognizable by their shape. Indeed, towns, rivers or crops are familiar shapes that are easily recognizable. Visually comparing the images that were taken 10 years apart, it reveal that new shapes have emerged.

Moreover, **Figures 33 (a) to 40 (a)** and the different tone (from black to white) helps learning more about vegetation and soil moisture content. Black represents water or crops with high moisture content as white features represent crops. Visually comparing the images of 2006 and 2016 confirms that the tone has changed all over. Some of the patches considered as crops have a different tone that suggests that there was change in the type of crops.

Indeed, as the images were taken at the same period, this shows that the vegetation might be of a different kind because their need in water is not the same at a given period: for example, corn might have replaced wheat.

Next, the spatial arrangement of objects in **Figures 33 (b) to 40 (b)** indicates that there was a change in the landscape structure in 10 years. In the different images, the spatial arrangement of patches considered as crops have changed. Some patches have appeared where there was none as others have disappeared.

Then, the resulting images of the algorithm suggests that there was a change in patches density. In **Figures 33 (b) to 40 (b),** the density of patches considered as crops globally tends to be higher in 2016 than in 2006. This suggests that the number of patches identified tend to increase over the years. However, contrasting **Figures 33 (b) to 40 (b)** does not help to discriminate the absolute sizes of patches considered as crops and its evolution over the years. However, the Landsat images and the results of the morphological operation provide information about the relative size of objects. The biggest patches are easily identifiable but further analysis is needed to determine the absolute size of objects.

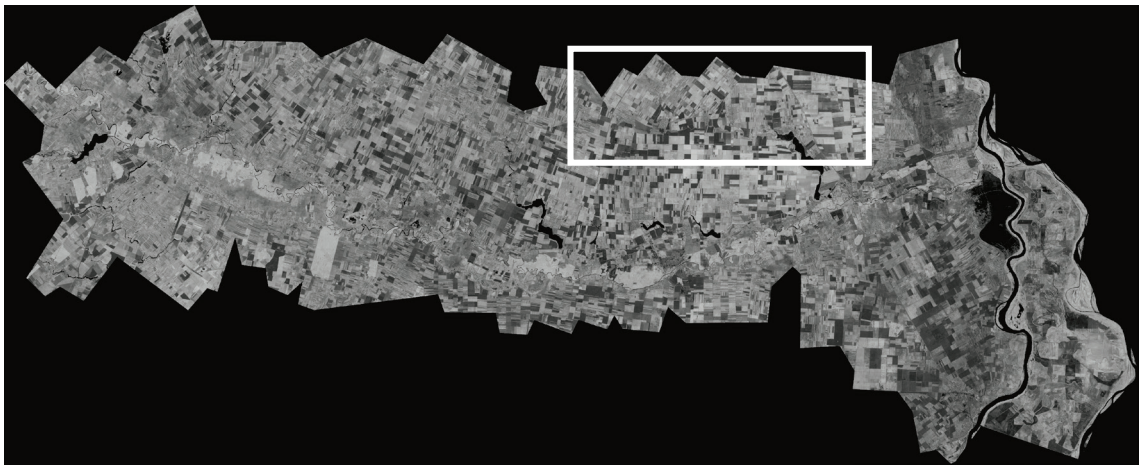

Figure 34. NDVI 2006. Ialomita County

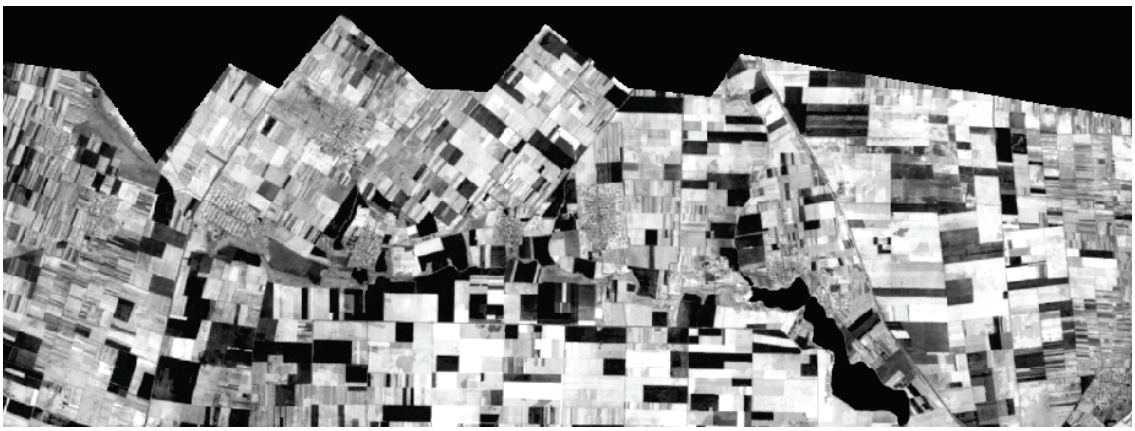

(a) Zoom on NDVI

(b) Zoom on morphological operation

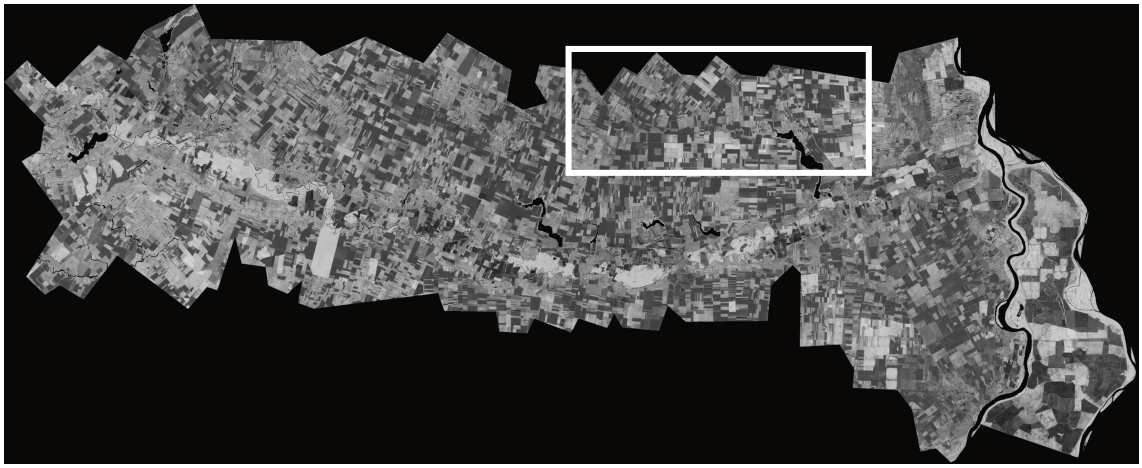

Figure 35. NDVI 2016. Ialomita County

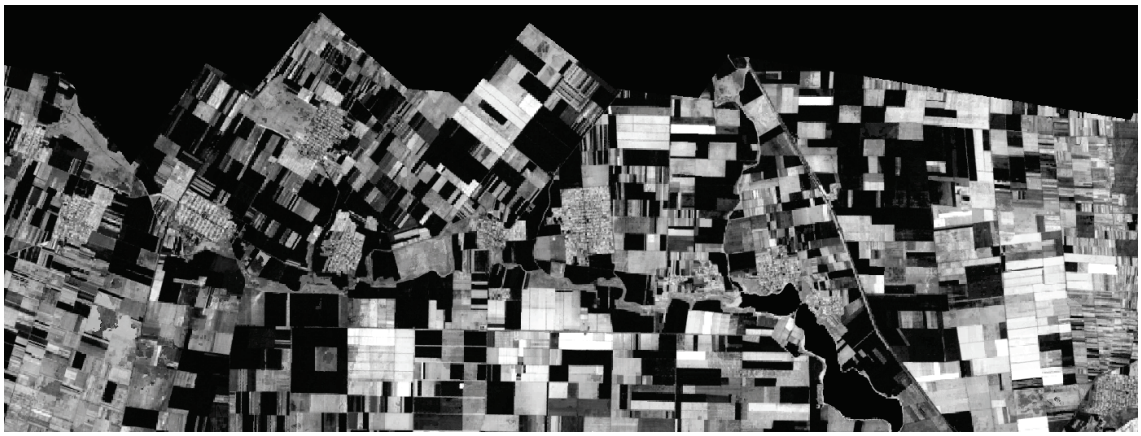

(a) Zoom on NDVI

(b) Zoom on morphological operation

Figure 36. Landsat 5 NDVI image 2006. Călăraşi County.

(a) Zoom on NDVI

(b) Zoom on morphological operation

Figure 37. Landsat 8 NDVI image 2016. Călărași County

(a) Zoom on NDVI

(b) Zoom on morphological operation

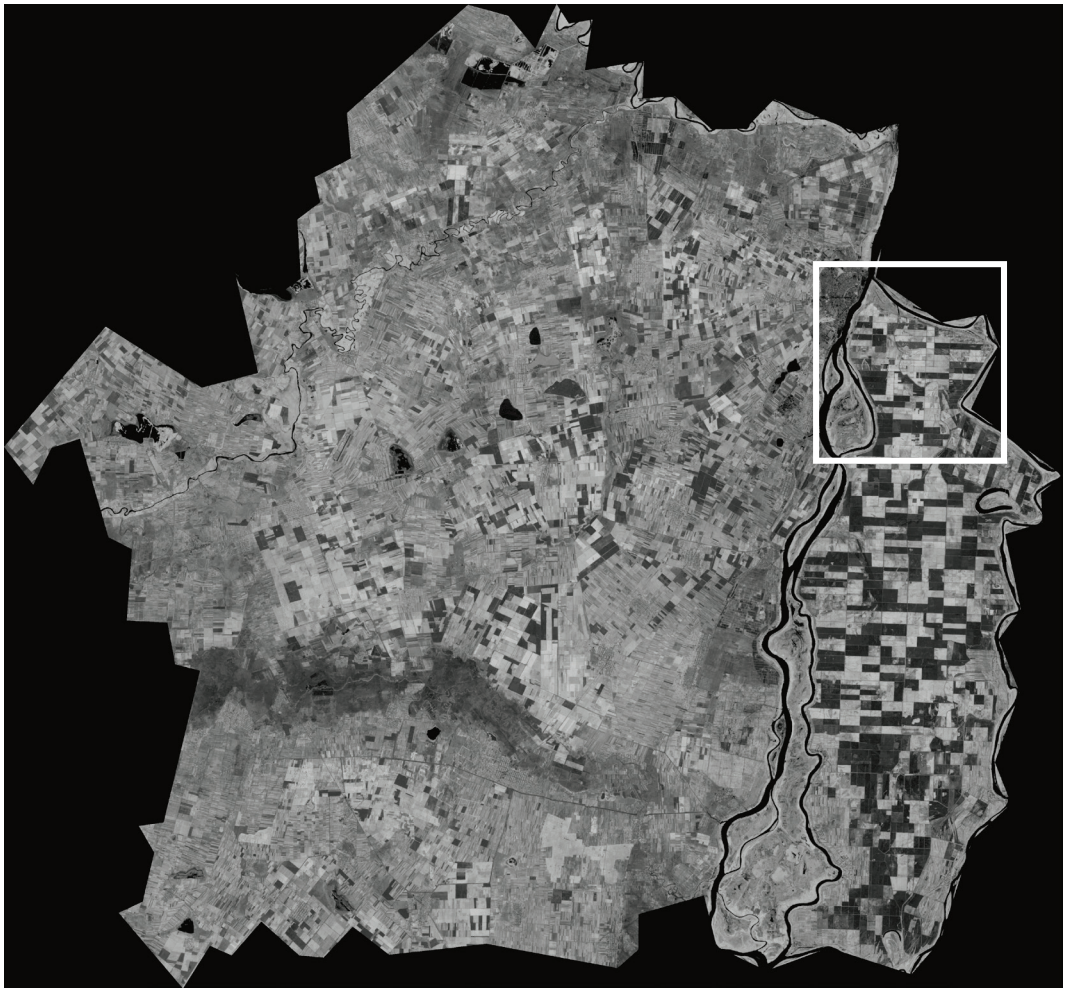

Figure 38. Landsat 5 NDVI image 2006. Brăila County

(a) Zoom on NDVI

(b) Zoom on morphological operation

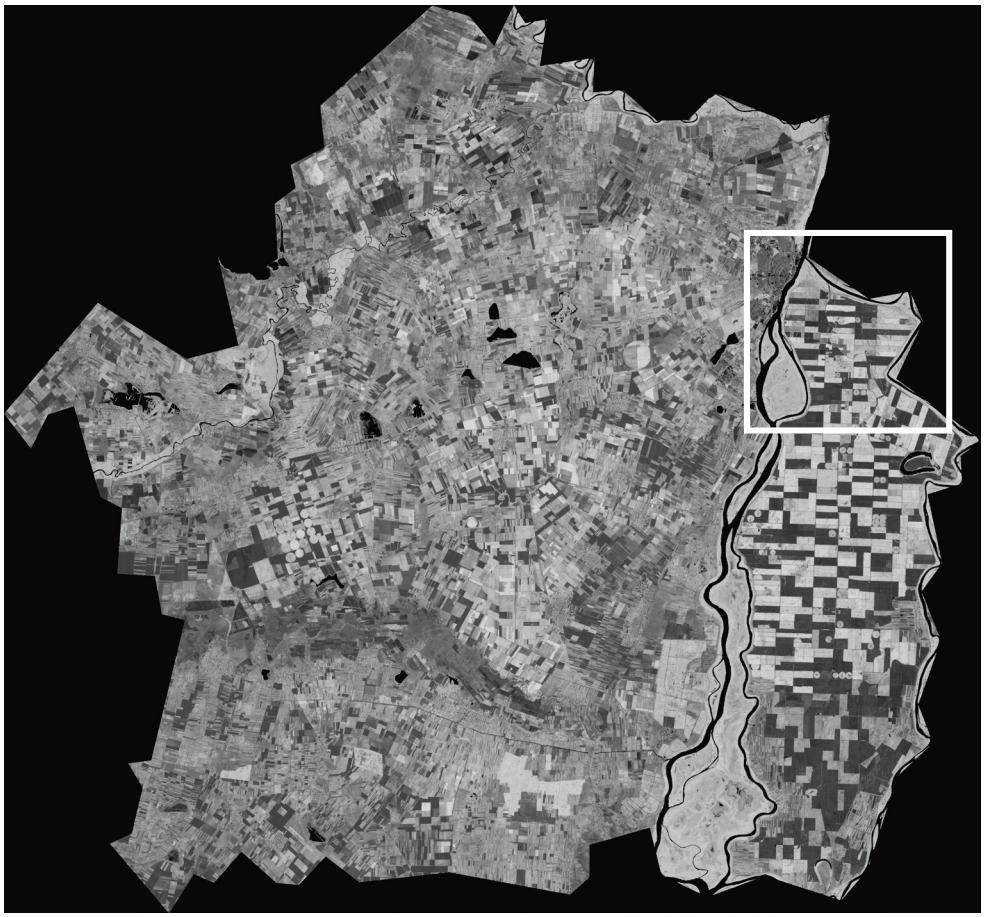

Figure 39. Landsat 5 NDVI image 2016. Brăila County

(a) Zoom on NDVI

(b) Zoom on morphological operation

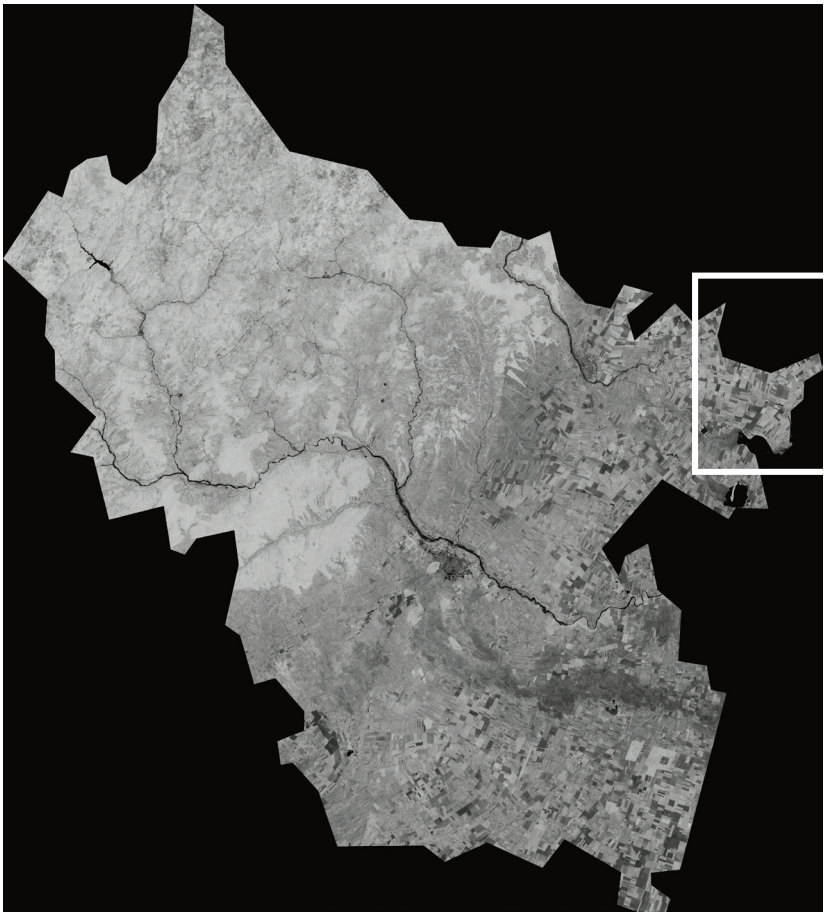

Figure 40. Landsat 5 NDVI image 2006. Buzău County

(a) Zoom on NDVI

(b) Zoom on morphological operation

Figure 41. Landsat 5 NDVI image 2016. Buzău County

(a) Zoom on NDVI

(b) Zoom on morphological operation

Histogram of size of patches of crops for 2006 – 2011 – 2016

Here, we implemented a histogram of the sizes of patches of crops that were identified by the algorithm. Following Bauer, Duffy & Westcott (2006) a histogram is a *"graphic representation (bar chart) used to plot the frequency with which different values of a given variable occur.* Data of the year 2011 exceptionally appears for the graphic representation to be more relevant.

Figure 42 provides an estimation of the fluctuation of the sizes of crops over the years when considering all sorted data. Comparing the results for the study areas, it suggests that the application of the algorithm results in lower frequencies of patches above the size of 50 hectares. In other words, there is a predominance of small-scale farming over the years. However, it seems that since 2006, there is a decrease in the number of patches that are considered to as small. Then, there are still about seven times more patches that could be considered as small as large crops. Finally, for the four counties studies, it does not seem that the 2016 dataset has values that are relatively different than the ones of the other years, especially when the graphic representation is dominated by the values under 50 hectares. The results obtained with this graphic representation make it impossible to identify differences of frequencies between the three years and also to interpret a possible evolution in the sizes of patches considered as crops.

Figure 42. Histogram of all patches with a) Ialomita b) Călărași c) Brăila d) Buzău

a)

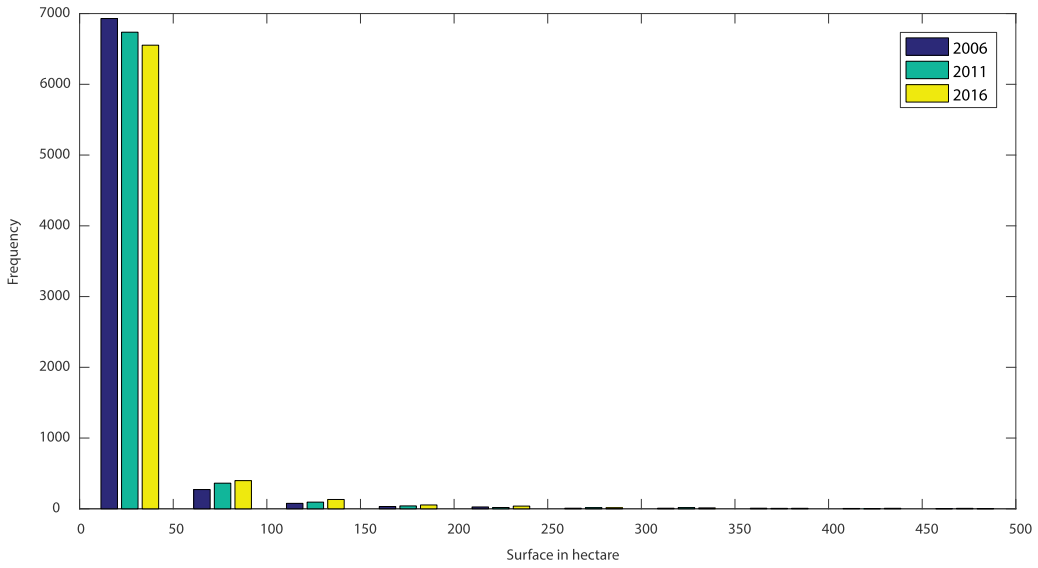

b)

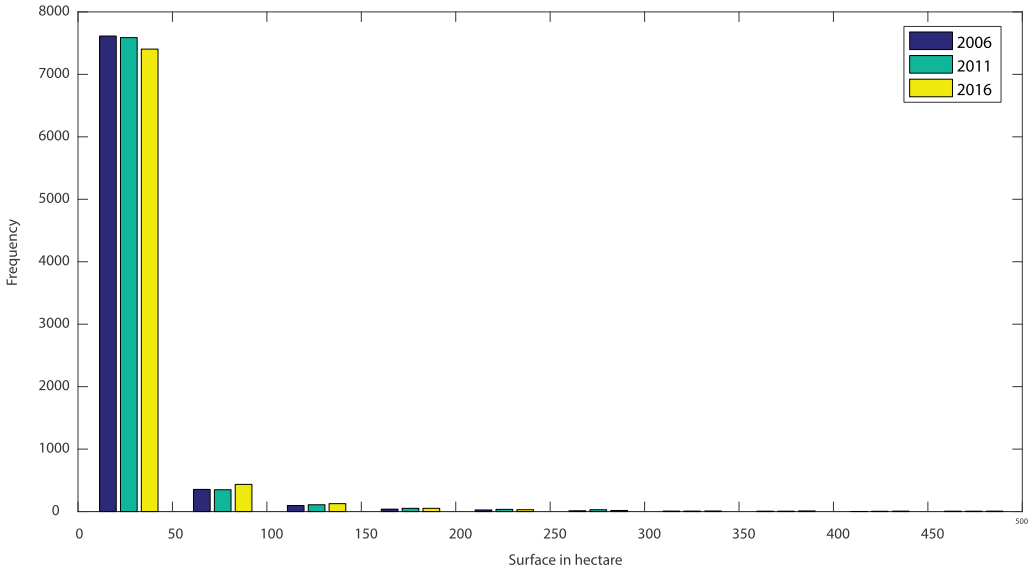
2006
2011
2016
Frequency
Surface in hectare
0
1000
2000
3000
4000
5000
6000
7000
8000
0
50
100
150
200
250
300
350
400
450
500

c)

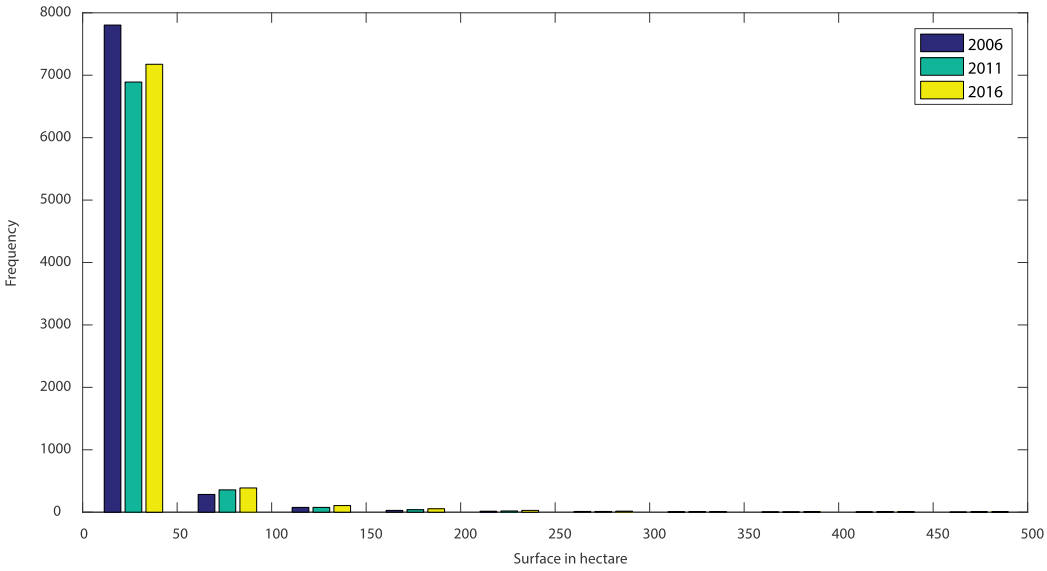
2006
2011
2016
Frequency
Surface in hectare
0
1000
2000
3000
4000
5000
6000
7000
8000
0
50
100
150
200
250
300
350
400
450
500

d)

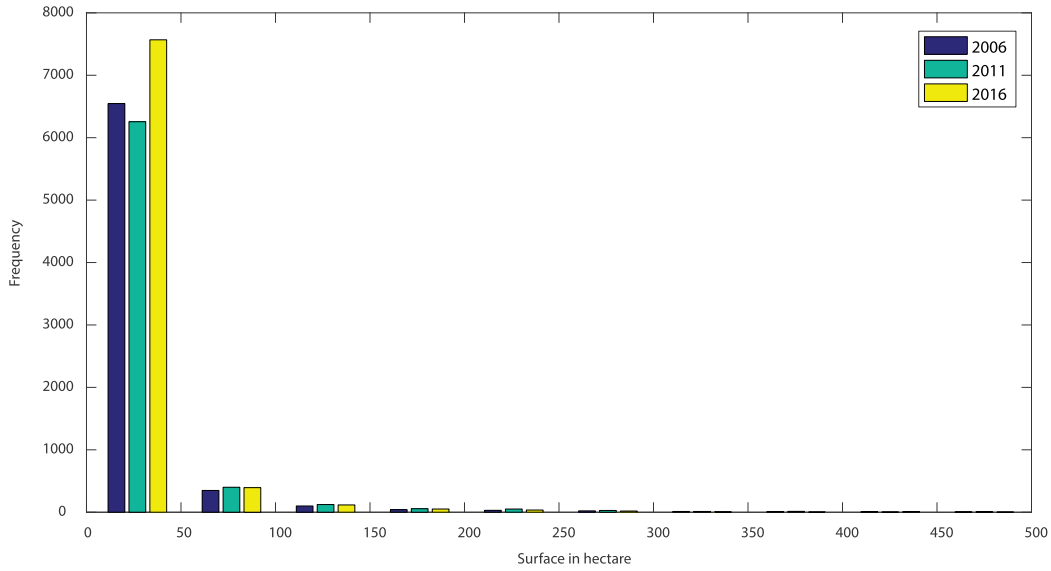
2006
2011
2016
Frequency
Surface in hectare
0
1000
2000
3000
4000
5000
6000
7000
8000
0
50
100
150
200
250
300
350
400
450
500

Figure 43 shows semi-log plot of all data. Semi-log plot is used because there were several values in the dataset, and we wanted to eliminate the scaling effects and to compare values between the different years. Indeed, here our main aim is not to see if there are more bigger producers than small producers at a given time, but to see local trends for a specific class of patches over the years.

It appears that the application of the algorithm results in lower frequencies of patches above the size of 100 hectares. Overall, in these histograms between 2006 and 2016 and for the 10 classes, the frequency tends to be higher for the year 2016 than for the previous years. However, for the four different counties, there are classes where the frequency is higher in 2010. A special situation may have occurred for these classes, but without a deeper knowledge of the local situation, using studies involving fieldwork it is not possible to explain these fluctuations.

Figure 43. Semi-log representation of all patches with a) Ialomita b) Călărași c) Brăila d) Buzău

a)

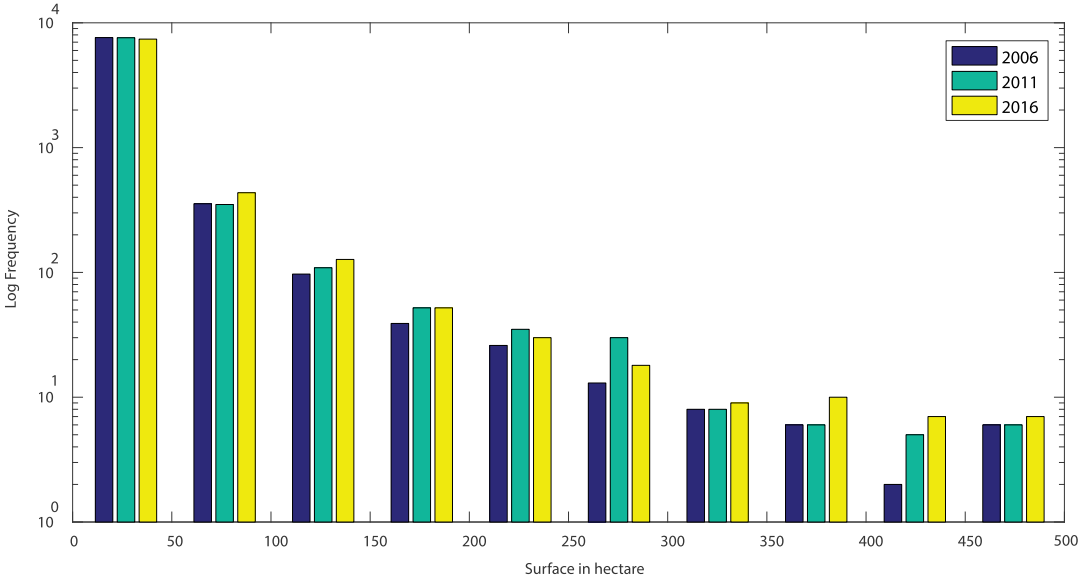

b)

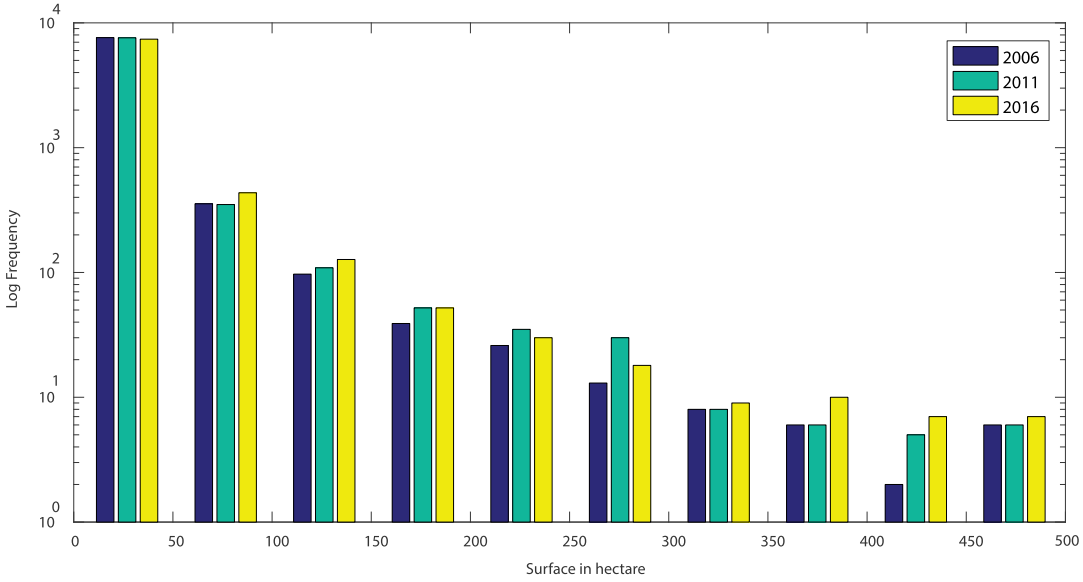
2006
2011
2016
Log Frequency
Surface in hectare

c)

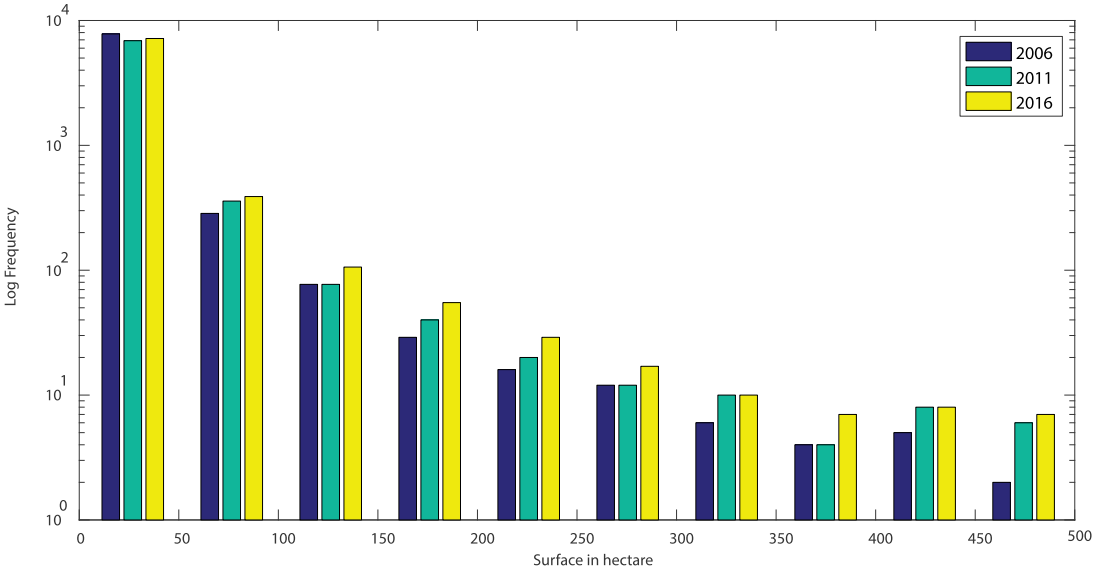
2006
2011
2016
Log Frequency
Surface in hectare

d)

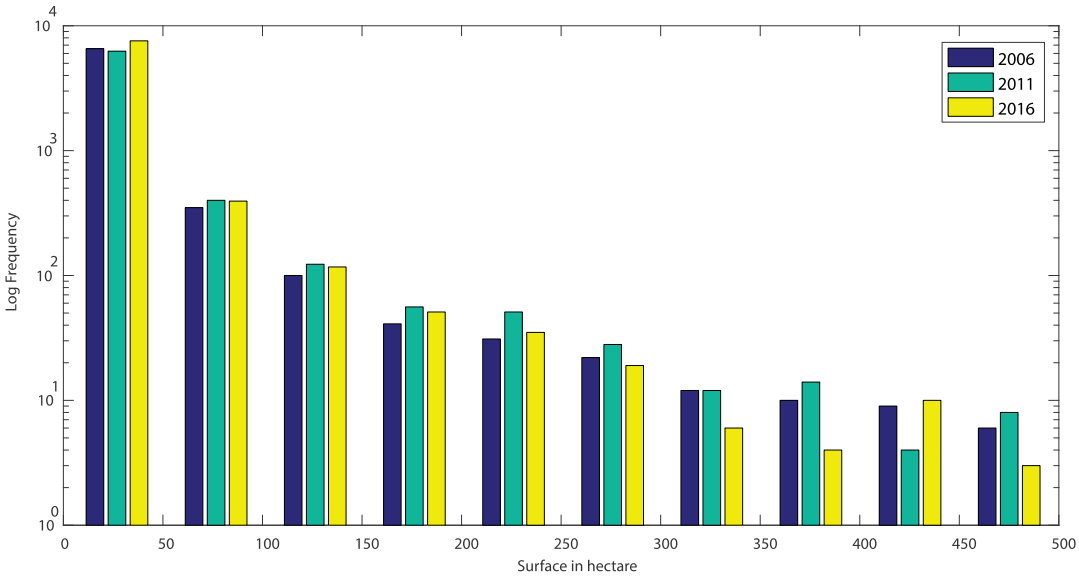
2006
2011
2016
Log Frequency
Surface in hectare

As explained below, the local tendencies that were detected with the 10 classes histogram may not be possible to explain without studies involving fieldwork, and in this work, this is not our aim.

Different and further analysis is actually needed; a histogram with three classes that go along with the three classes suggested by the EU was implemented. In short, the number of bins were decreased in order to highlight the essential changes. **Figure 44** illustrate the histogram of small, medium and large patches (2 -20, 20-100 and 100 to 500 hectares) for the four areas of interest and for the years 2006-2011-2016.

It turns out at that for the four study areas, the application of the algorithm results in an evolution of the frequencies of small, medium and large patches over the years. Overall, the general tendency of these histograms is that between 2006 and 2016, the frequency of medium sized and large patches tends to be higher. On the contrary, these figures suggests that the frequency of small patches tends to be lower. This figure indicates that if there is an evolution of the frequencies of small, medium and large patches considered as crops that might by implied by land grabbing, it is confirmed by this figure. However, in the **Figure 44 (d),** the county of Buzău seems to have a trend that is different from the others.

Figure 44. Medium and large patches in a semi-log representation with a) Ialomita b) Călărași c) Brăila d) Buzău.

a)

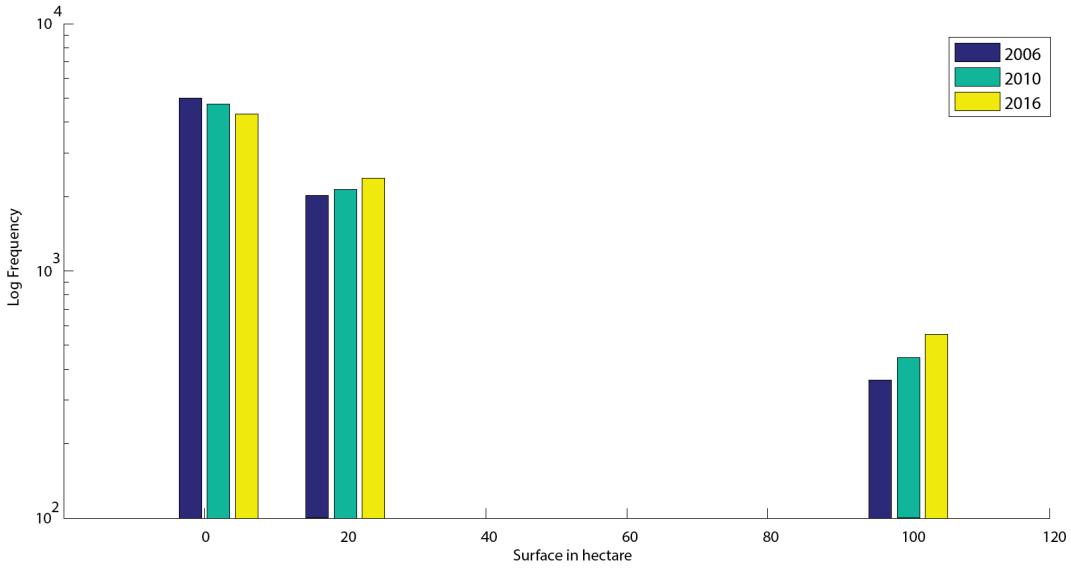

b)

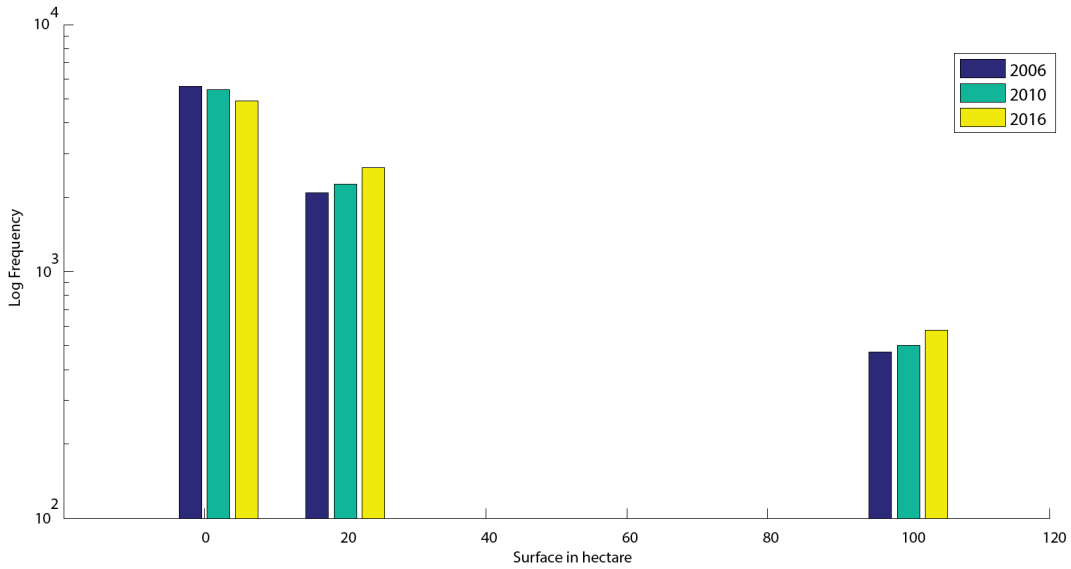
2006
2010
2016
Log Frequency
Surface in hectare
0
20
40
60
80
100
120

c)

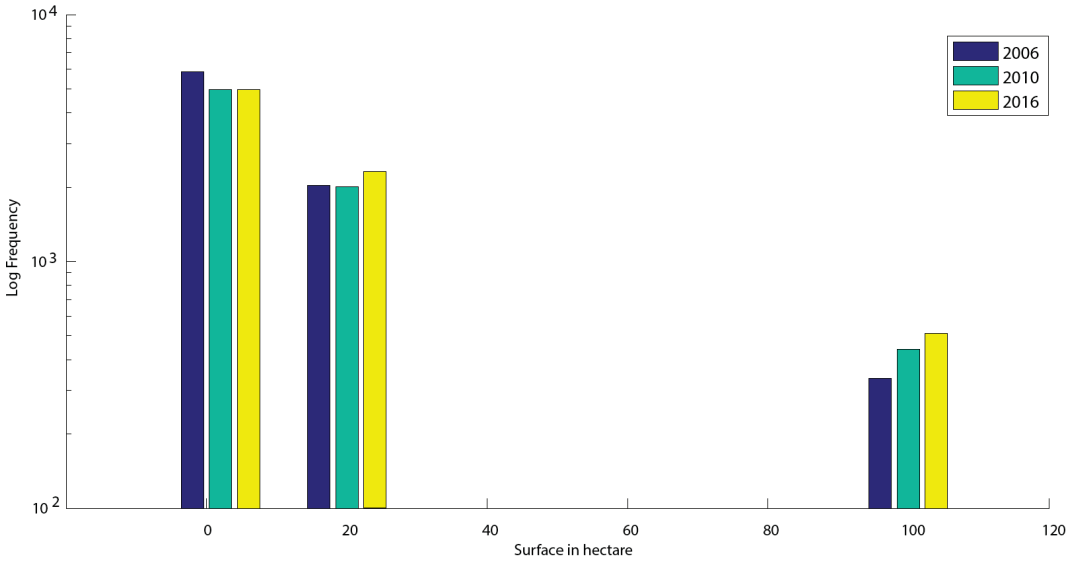
2006
2010
2016
Log Frequency
Surface in hectare
0
20
40
60
80
100
120

d)

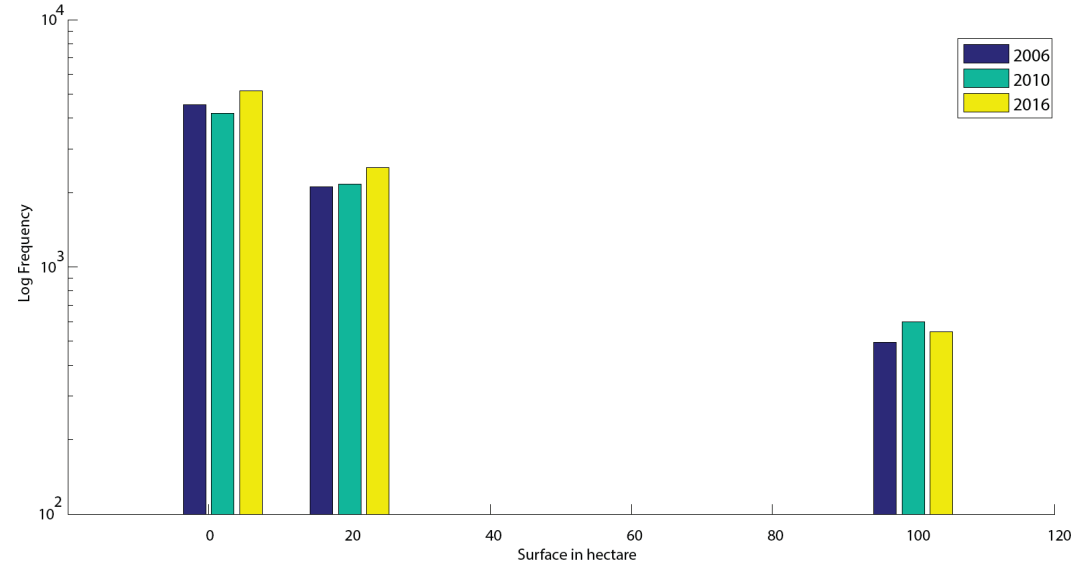
2006
2010
2016
Log Frequency
Surface in hectare
0
20
40
60
80
100
120

General evolution of patches statistics

In the section, we computed some statistical results from the sorted data. The histograms computed in the previous section show the differences in frequency for various classes and between three periods. However, these frequencies do not give information about the percentage of large, medium or small patches, and how this percentage has evolved over the years.

Table 3 sums up the number of large patches for the period we are interested in. It seems that their number tend to increase over the years and for every place of interest. Looking at the percentage, it seems to vary over the years and with an increase of about 30 %. The results of the county of Buzău suggest that its trend is a little bit different from the others with a weaker increase.

	Evolution of large-sized patches							
	Ialomita		**Călărași**		**Brăila**		**Buzău**	
	2006	**2016**	**2006**	**2016**	**2006**	**2016**	**2006**	**2016**
Number	172	271	199	268	155	242	241	248
Percentage	2.3 %	3.7 %	2.7 %	3.6 %	2.1 %	3.3 %	3.3 %	3.4 %

Table 3. Statistics about large-sized patches (< 100 hectares)

Table 4 displays the number of patches classified as medium-sized patches. Over the years, it seems that their number tends to increase for the four counties. Then, over the years, there is a general increase of the percentage. By contrast, with large-sized patches in **Table 3,** the number and percentage of medium-sized patches seems to have a weaker increase. This suggest that the size of large patches is more likely to increase than the medium-size patches.

	Evolution of medium-sized patches							
	Ialomita		**Călărași**		**Brăila**		**Buzău**	
	2006	**2016**	**2006**	**2016**	**2006**	**2016**	**2006**	**2016**
Number	1133	1570	1292	1702	1209	1416	1354	1573
Percentage	15.4 %	21.7 %	17.5 %	21.0 %	16.4 %	18.1 %	18.4 %	19.2 %

Table 4. Statistics about medium-sized patches (20 < x <100)

Both the increase of the percentage of large and medium-sized patches may suggest that there was a decrease in the percentage of the patches identified as small. **Table 5** suggests that. There is indeed a general decreased in the number and in the percentage of small-sized patches from 2006 to 2016, except for the county of Buzău where there is an increase of about 10%.

	Evolution of small-sized patches							
	Ialomita		**Călărași**		**Brăila**		**Buzău**	
	2006	**2016**	**2006**	**2016**	**2006**	**2016**	**2006**	**2016**
Number	6064	5379	6675	6130	6876	6146	5532	6386
Percentage	82.3 %	73.0 %	90.6 %	83.2 %	93.3 %	83.4 %	75.1 %	86.7 %

Table 5. Statistics about small-sized patches (2 < x < 20)

It comes out at that for the four study areas the application of the algorithm results in an evolution of the frequencies of small, medium and large patches over the years. The general tendency of these statistics is that between 2006 and 2016, the number and the percentage of large-sized patches has a strong increase. Then, concerning medium-sized patches, it comes out that there was a general increase as well. Small-sized patches are more likely to decrease. However, the statistics about the county of Buzău seems to infer the contrary.

The images processing and image segmentation tends to lead to a constant and general trend: the increase of large-sized patches as the decrease of small-scale patches. If there is predominance of this fact, it is confirmed by **Table 6**. It shows the total number of areas classified as patches of crops in 2006 and 2016. There is a variability between the two years and for the four counties. Globally, the total number of patches classified as crops has decreased after 10 years for all counties but increased for the county of Buzău.

The total area of all vectors classified as patches of crops is also displayed. Unusually, the total area for the four counties is largely superior in 2016 than in 2006. This is even if the total number of areas classified tends to be smaller over the years.

This suggest that even if the number of patches identified as crops have decreased in 10 years; the total surface in use has increase. Overall, this general tendency may bring in mind that large-sized land acquisition have been made these past few years.

Evolution of the statistics about patches identified as crops by GEE

	Ialomita		**Călărași**		**Brăila**		**Buzău**	
	2006	**2016**	**2006**	**2016**	**2006**	**2016**	**2006**	**2016**
Number	7369	7220	8166	8100	8240	7804	7127	8207
Total area in hectare	118’350	151’890	134’720	164’200	120’420	148’650	141’860	155’460

Table 6. Evolution of the statistics about all patches identified as crops

V. Discussion

The aim of this work was to assess land grabbing by putting forward the hypothesis that land grabbing implies large-scale land deals and that the evolution of the size of the patches considered as crops is related to land grabbing. This work has shown that satellite imagery and the methodology that was implemented based on image segmentation in the Google Earth Engine platform were able to identify object-based features. Moreover, the identification went along with statistical values of these objects, such as their size.

Histograms and statistics about objects-based features provided by the algorithm has led to interesting and contrasting results about the evolution of the size of the patches over the years. Particularly, the decrease of small patches compared to the increase of medium and large-sized patches. Images analysis suggested that for the different study areas, there was an evolution of the landscape arrangement although a quantitative approach was not possible.

To go further and verify the data that were acquired, we associated the empirical values obtained by the proposed methodology with official statistics from the National Institute of Statistics of Romania. The trend that we obtained from our data was confirmed, as their numbers infer a similar tendency. Although the tendency is similar, the values are not the same and the difference is obvious. Our algorithm computed values that are about two times lower than the official statistics. However, the trend seems to be scientifically relevant because the bias is constant throughout the different tables and more specifically, where the official number sees an increase, the empirical number sees an increase, too. This being said, the results of the county of Buzău are very different from the results of the other counties. The results have shown that in this county, there was an increase of small patches with a decreased of the two other categories. Where the official statistics see a decrease, we see an increase in the total land dedicated to agriculture. In this county, the differences between official and empirical number are also closer than in the others counties.

Differences with official statistics, differences in the results of one county and the general trend might suggest interesting conclusions about this tendency as well as possible uncertainties and limits to this methodology.

	Differences between official agricultural statistics and empirical statistics (total land dedicated to agriculture)							
	Ialomita		**Călărași**		**Brăila**		**Buzău**	
	2006	**2016**	**2006**	**2016**	**2006**	**2016**	**2006**	**2016**
Official number	317’213	349’927	374’255	394’165	294’258	376’762	247’808	257’870
Empirical number	136’640	162’720	154’790	187’630	136’380	161’650	226’460	195’530
Difference	43.1	46.5	41.4	47.6	46.3	42.9	91.4	75.8

Table 7. Official statistics and empirical statistics (total land dedicated to agriculture in hectares)

The general tendency in the results may bring to mind that large-scale land acquisition has been made these past few years in Romania. Indeed, following Ecoruralis (2016), from 2002 to 2010, 150,000 small farms have disappeared in Romania while the number of large farms has increased by 3%. In this country, there have been crucial changes regarding land allocation and agriculture these past few decades. This general tendency can also instructs us about different form of agriculture that might coexist: family agriculture in small-scale patches or intensive agriculture on large-sized patches. Nevertheless, land grabbing exhibits complex dynamics and undoubtedly, it cannot be only explained using the images, number and statistics obtained by the proposed methodology. The different trends in the county of Buzău should also be taken into account.

Furthermore, this evolution in the landscape structure may not only be related to land grabbing. Following Zoomers (2010), land grabbing is not the only process to be hold responsible for the radical changes in landownership and land use throughout the whole world; large-scale tourist complexes, foreign direct investment in non-food agricultural commodities and biofuels are other causes. Eventually, the different counties that were analyzed might have different local dynamics.

Next, uncertainties of the proposed methodology are highlighted by comparisons with the official statistics. Several leads are possible. The different parameters of the algorithm were selected based on best-fitting visual results. This means that for each step of the methodology that was proposed, several parameters values were tested. The extreme values that led to irrational results were implemented first. Then, those values were systematically filtered. This process was repeated until the visually best segmentation and visually best morphological operation result was obtained. However, with a validation process of parameters, the results might have been closer to reality, at least different.

Moreover, the differences with the official statistics is one thing, but the evolution of the empirical numbers over the years is another. The satellite imagery comes from two different satellites. Indeed, the change detection period and the problem of Landsat 7 SLC failure has been a challenge. This might have influenced the results. Indeed, two different satellite imageries from Landsat 5 and Landsat 8 were used and despite using the correct band correspondence, Landsat 5 imagery processing resulted in noisier results. The algorithm parameters that were implement had the same values, which can bring difficulties of interpretation. In short, the results obtained when performing our methodology on two different Landsat images might have been a little bit different when performed with the same satellite.

Then, some limits to the study exist. First, as a cloud-free software, Google Earth Engine has a limited computation capacity. This means that we were not able to assess land grabbing for the whole Romania without implementing vector data of every county. This led to time-consuming work of importing vector data into the interface. Then, the classification algorithm provided by Google Earth Engine appeared to not be accurate enough to build our work on. Several classifications were done but this could not be the primary reference of our work. Hence, raster data of land cover had to be implemented which prevented us from further assessing land grabbing everywhere else.

However, some positive arguments do emerge. Instead of using classical tools such as Erdas Imagine or Matlab, amongst others, Google Earth Engine was used for this work. This cloud platform that was launched in 2010 proved to be a very convenient tool. In other words, no downloading of images were needed and there were thousands of freely available satellite images. This may have helped in the choice of the best image available. In addition, many algorithms are provided in this platform as well as well-shaped documentation and tutorials. This appeared to be very useful in learning to use this platform.

Finally, this Master thesis provides possibilities for improvements for future work. Google Earth Engine has various computation skills and freely available satellite imagery that were not investigated. For example, European Space Agency has launched various satellites those past few years and "*the Sentinel-2 mission is a land-monitoring constellation of two satellites that provide high-resolution optical imagery and provide continuity for the current SPOT and Landsat missions"* (European Space Agency, 2018). Google Earth Engine provides growing collection of Sentinel-2 data and this seem to be a very interesting for further researches on land grabbing. However, this satellite was launched in 2015; therefore, long-term perspective may be a challenge.

As stated above, classification algorithms provided by Google Earth Engine did not seem accurate enough to build our work on it. Hence, assessing land grabbing everywhere else than in Romania or in country where land use raster exists is restricted. For further investigations on land grabbing in countries outside of European Union, developing efficient classification algorithms appears to be appealing. Considerations are required to perform this complex process like *"determination of a suitable classification system, selection of training samples, image preprocessing, feature extraction, selection of suitable classification approaches, post-classification processing, and accuracy assessment"* (Lu & Weng, 2007, p. 824). However, this is a challenge that may be addressed for future work on this topic.

Best-fitting visual results allowed us to select the different parameters of the algorithm. Parameters validation appears to be interesting in obtaining better and more accurate results of the evolution of the landscape structure based on image segmentation. Indeed, object-based image analysis depends on image segmentation (Costa, Foody, & Boyd, 2018). An in-depth examination should be given on the opportunities to perform parameters validation when using Google Earth Engine.

Altogether, technical requirements associated with the use of a new software and related to the implementation of an algorithm, image and numerical results interpretation were challenging Furthermore, linking relations between the results and the topic of land grabbing, in other words, linking people to pixels is difficult. As stated by Entwisle, Moran, Rindfuss, Turner & Walsh (2012 , p. 387), *"there is no necessary parallel between social units and land units. Moreover, coverage of one does not necessarily guarantee coverage of the other"*. Combining different field of study such as remote sensing, land grabbing, sustainable development and human rights is complex. This question undoubtedly needs to be addressed but this is surely an interesting insight for futures researches not only for the topic of land grabbing but also for other land change issues.

VI. Conclusion

This Master thesis included image segmentation, morphological operation and vectors extraction based on a new cloud platform called Google Earth Engine. The proposed methodology was implemented on Landsat imagery, for four different places across Romania and for two different years. The proposed method has shown that preprocessing and processing of images is mandatory

The results proved that the method that was implemented was able to identify object-based features. The proposed work also provided good results knowing that the parameters of the algorithms were chosen on best-fitting visual results and that Google Earth Engine is a relatively new platform. This process yield patches considered as crops very close to Landsat images and good results in assessing changes in spatial arrangements of these patches. It also clearly shows an evolution of the sizes of the patches considered as crops over the years with globally a decrease of small-scale patches and increase of large-scale patches. This evolution yielded to new insight into land grabbing in Romania.

However, Google Earth Engine was able only to detect patches of crops from Landsat 5 and Landsat 8 imagery with the help of a land cover raster. Hence, this methodology works when there is a classification layer below. Without this classification, the algorithm would not have been able to detect the patches therefore; there is a need to train a classifier. The results showed the potential use of Google Earth Engine imagery but also revealed some limitations of this platform.

Although, this Master thesis provides possibilities for improvements and interesting insights for the future. Coupled with field studies, parameters validation, high quality images as well as automatic classification, this method may be interesting in helping assessing land grabbing and prevent further damages like environmental damages, exploitation of workers and illegal transactions not only in Romania but also in other countries.

VII. References

Angalaparameswari , R., & Senthilkumar, P. (2014, February). Image denoising using median filter with edge detection using canny operator. *International journal of science and research, 3*(2).

Bauer, J., Duffy, G., & Westcott, R. (2006). *The Quality improvement handbook.* Milwaukee, Wisconsin : ASQ Quality Press .

Borras, J., Scoones, I., & Hughes, D. (2011, Avril 15). Small-scale farmers increasingly at risks from global land grabbing . *The Guardian* .

Bourgeois, L. (2009, March). La sécurité alimentaire à l'épreuve des crises financières et économiques . *Pour, 202-203*, pp. 26-37.

Boyle, R., Sonka, M., & Hlavac, V. (1993). *Image pre-processing. In: Image Processing, Analysis and Machine Vision.* Boston: Springer.

Brunner, S., Grêt-Regamey, A., & Stritih, A. (2016). Landscape : structural approach . (D. o. ETH, Ed.) Zürich, Switzerland.

Campbell, J., & Wynne, R. (2011). *Introduction to Remote Sensing* (5th edition ed.). New York, USA: Guilford Press.

Campbell, J., & Wynne, R. (2011). *Introduction to remote sensing. Fifth edition.* Guilford Press .

Canty, M. J. (2010). *Image Analysis, classification, and change detection in remote sensing.* CRC Press.

Claverie, B. (2013, March). Le blé, enjeu de la sécurité alimentaire chinoise. *Géoéconomie, 66*, pp. 83-100.

Colstoun, E. B. (2010). *The electromagnetic spectrum* . Retrieved December 26, 2017, from https://science.nasa.gov/ems/08_nearinfraredwaves

Costa, H., Foody, G., & Boyd, D. (2018, February). Supervised methods of image segmentation accuracy assessment in land cover mapping. *Remote Sensing of Environment, 205*, pp. 338–351.

Cotula, L., Keeley, J., Leonard, R., & Vermeulen, S. (n.d.). *Land grab or development opportunity ? Agricultural investment and international land deals in Africa* . IEED/FAO/IFAD, London.

De Morsier, F. (2016). Information Extraction - Segmentation. Imagery of territory.

Dufumier, M., & Hugon, P. (2008). PIQUES ET POLÉMIQUES LES « ÉMEUTES DE LA FAIM » : DU SOUS INVESTISSEMENT AGRICOLE À LA CRISE SOCIOPOLITIQUE. *Revue Tiers Monde, 196*(4), pp. 927-934.

Ecole Nationale des Sciences Géographiques. (2013, May 15). *Les bases de l'Information Géographique*. Retrieved December 30, 2017, from L'essentiel de la géomatique : http://www.ente-aix.fr/documents/118-demoGeo/demo/4_BasesIG/co/20_gr_PubliRasterVecteur.html

Entwisle, B., Moran , E., Rindfuss, R., Turner , B., & Walsh, S. (2012). *Linking Pixels and People. In: Gutman G. et al. (eds) Land Change Science. Remote Sensing and Digital Image Processing* (Vol. 6). Dordrecht: Springer. doi:https://doi.org/10.1007/978-1-4020-2562-4_22

European commission's directorate general for agriculture and rural development. (2017, September 10). *CAP at glance*. Retrieved October 8, 2017, from Agricultural and rural development: https://ec.europa.eu/agriculture/cap-overview_en

European Space Agency. (2018). *What is Sentinel-2?* Retrieved January 2, 2018, from Earth online: https://earth.esa.int/web/guest/missions/esa-operational-eo-missions/sentinel-2

European Union . (2017, September 8). *Small and large farms in the EU - statistics from the farm structure survey*. Retrieved from Eurostat - Statistics explained : http://ec.europa.eu/eurostat/statistics-explained/index.php/Small_and_large_farms_in_the_EU_-_statistics_from_the_farm_structure_survey

Franco, J., Peuch, J., & Kay, S. (2015). *Extent of farmland grabbing in the EU.* Brussels. Retrieved from http://www.europarl.europa.eu/RegData/etudes/STUD/2015/540369/IPOL_STU(2015)540369_EN.pdf

Girard, M.-C., & Girard, C. (1999). *Traitement des données de télédetection* . Paris : Dunod.

Giuşcà, B. (2005 , December 21). *Romanian counties map* . Retrieved December 22, 2017, from https://commons.wikimedia.org/wiki/File:Romania-administrative-blank-large.png

Google Developers . (2017, October 31). *Google Earth Engine API*. Retrieved January 2, 2018, from Edge detection: https://developers.google.com/earth-engine/image_edges

Google Developers. (2017, October 31). *Google Earth Engine API*. Retrieved January 05, 2018, from Landsat Algorithms : https://developers.google.com/earth-engine/landsat#simple-composite

Gorelick, N., Hancher, M., Dixon, M., llyushchenko, S., Thau, D., & Moore, R. (2017, July 6). Google Earth Engine : Planetary-scale geospatial analysis for everyone. *Remote sensing of environment*, p. 10.

Grazzini, J., & Soille, P. (2009). Edge-preserving smoothing using a similarity measure in adaptive geodesic neighbourhoods . *Pattern Recognition, 42*, pp. 2306 - 2316.

Hoster, P., Kuemmerle, T., St-Louis, V., & Radeloff, V. (2009, March). Using image texture to map farmland field size : a case study in Eastern Europe. *Journal of land use science, 4*(1-2), pp. 85-107.

International Land Coalition . (2012). *Annual report 2011*. Rome: International fund for agricultural development .

International land coalition. (2011). *Annual report* . Rome.

Knight, D. (2010). *Romania and the common agricultural policy.* University of Denver, Colorado, USA.

Land Matrix Global Observatory. (2017). *Global map of investments*. Retrieved December 22, 2017, from Land Matrix : http://www.landmatrix.org/en/get-the-idea/global-map-investments/#

Lillesand, T., Kiefer, R., & Chipman, J. (2015). *Remote sensing and image interpretation* (7th edition ed.). Hobocken, NJ, USA: Wiley & Sons .

Lu, D., & Weng, Q. (2007, March 10). A survey of image classification methods and techniques for improving classification performance. *International journal of Remote Sensing, 28*(5), pp. 82-870.

Magdoff, F. (2013, November). Twenty-first-century land grabs. Accumulation by agricultural dispossession. *Monthly review, 65*(6).

Morse, B. (2000, February 12). *Lecture 13 : Edge detection* . Retrieved December 27 , 2017, from http://homepages.inf.ed.ac.uk/rbf/CVonline/LOCAL_COPIES/MORSE/edges.pdf

NASA. (1999). *Ask a scientist*. Retrieved November 5, 2017, from Earth observatory. Where every day is earth day: https://earthobservatory.nasa.gov/Features/AskScientist/askscientist_6.php

NASA. (2012, October 14). *What are passive and active sensors ?* Retrieved December 26, 2017, from https://www.nasa.gov/directorates/heo/scan/communications/outreach/funfacts/txt_passive_active.html

NASA. (2017, December 21). *A Landsat timeline* . Retrieved December 26, 2017, from https://landsat.gsfc.nasa.gov/a-landsat-timeline/

NASA. (2017, November 7). *Electromagnetic spectrum diagram*. Retrieved December 26, 2017, from https://mynasadata.larc.nasa.gov/science-practices/electromagnetic-diagram/

Pawar, S., & Banga , V. (2012). Morphology Approach in Image Processing. *International Conference on Intelligent Computational Systems* , (pp. 158-150). Dubaï.

Roger-Machart, Y. (2009, Mars). Les grands investissements fonciers agricoles au niveau international. *Pour, 202-203*, pp. 149-157.

Rouillé d'Orfeuil, H. (2009, March). Faire face aux besoins alimentaires, la question des consommateurs pauvres ou insolvables. *Pour, 202-203*, pp. 64-72.

Sch. (2006, June 9). *Black body spectrum Loglog*. Retrieved December 22, 2017, from https://commons.wikimedia.org/wiki/File:BlackbodySpectrum_loglog_150dpi_en.png

SEOS Project . (2017). *Introduction of categorisation of objects from their data*. Retrieved December 26, 2017, from http://www.seos-project.eu/modules/classification/classification-c01-p05.html

Serra, J. (1982). *Image Analysis and mathematical morphology* (Vol. 1). Londres: Academic press.

Serra, J. (1988). *Image analysis and mathematical morphology* (Vol. 2). Londres: Academic Press.

Soille, P. (2000). Morphological image anlaysis applied to crop field mapping. *Image and Vision Computing, 18*, pp. 1025-1032.

Spoor, M., & Visser, O. (2011). Land grabbing in post Soviet Eurasia : the world's largest agricultural land reserve at stake. *Journal of peasants studies, 38*(2), pp. 299-323.

Sweeney, M. (2009, September 25). Retrieved December 26, 2017, from https://pixabay.com/en/puzzle-game-solution-connection-226743/

U.S Navy. (2006, January 31). *Atmosfaerisk spredning*. Retrieved December 22, 2017, from https://commons.wikimedia.org/wiki/File:Atmosfaerisk_spredning.png.

U.S. Geological Survey. (2017, June 22). *What are the band designations for the Landsat satellites?* Retrieved from USGS. Science for a changing world: https://landsat.usgs.gov/what-are-band-designations-landsat-satellites

Vigil, S. (2015, Avril). Une cause invisible des migrations : la trajedie de l'accaparement des terres. *Cités, 64*, pp. 111-124.

Zoomers, A. (2010, April). Globalization and the foreignization of space : seven processes driving the current global land grab. *The journal of peasants studies, 37*, pp. 429-447.

VIII. Annexes

1. Algorithm code used in Google Earth Engine

```
// Load a raw Landsat 8 or Landsat 5 orthorectified ImageCollection for an entire summer
var collection = ee.ImageCollection('LANDSAT/LT5_L1T')
    .filterDate('2006-07-01', '2006-09-01');
//Map.addLayer(collection);

// Create a cloud-free composite with default parameters.
var composite = ee.Algorithms.Landsat.simpleComposite(collection);

// Import raster layer of EU classification of 2006
var classification = ee.Image('users/myriameggerschwiler/g100_clc06_V18_5_Clip11');
 // Define visualization parameters to display the land cover map of 2006
var vizParams = {
  bands: ['b1'],
  min: 0,
  max: 255,};
var palette =
['#e6004d','#ff0000','#cc4df2','#cc0000','#e6cccc','#e6cce6','#a600cc','#a64d00','#ff4dff',
'#ffa6ff', '#ffe6ff','#ffffa8',
'#ffff00','#e6e600','#e68000','#f2a64d','#e6a600','#e6e64d','#ffe6a6','#ffe64d','#e6cc4d','#
f2cca6','#80ff00','#00a600',
'#4dff00','#ccf24d','#a6ff80','#a6e64d','#a6f200','#e6e6e6','#cccccc','#ccffcc','#000000','#
a6e6cc','#a6a6ff','#4d4dff',
'#ccccff','#e6e6ff','#a6a6e6','#00ccf2','#80f2e6','#00ffa6','#a6ffe6','#e6f2ff','#FFFFFF','#
FFFFFF','#e6f2ff'];
var ndwiViz = {min: 0, max: 255, palette: palette};

// Load the desired county of Romania from a Fusion Table.
var judet = Romania_Counties.filter(ee.Filter.eq('name', 'IalomiEa'));

// Load the land cover map of 2006 clipped with the county boundaries
var nl2012 = classification.clipToCollection(judet);
Export.image.toDrive({
  image: nl2012,
  description: 'LandCoverMap',
  scale: 30,
  region: judet,
  crs : 'EPSG:3857'
});
//Map.addLayer(nl2012, ndwiViz, 'Land cover map');

// Convert the 44 classes into vectors and filter the classes we are interested in (agriculture)
var vectors = nl2012.reduceToVectors({
```

```
  geometry : judet,
  bestEffort :true,
});
var points = vectors.filter(ee.Filter.gte('label', 12))
                .filter(ee.Filter.lte('label', 22));
var agriculture = nl2012.clip(points);
Export.image.toDrive({
  image: agriculture,
  description: 'LandCoverAgriculture',
  scale: 30,
  region: judet,
  crs : 'EPSG:3857'
});
//Map.addLayer(agriculture,[],'Land Cover agriculture');

// Clip the Landsat image with the bound of the classified image so the
computation on the NDVI layer is only made in the zone we are interested in
var clip = composite.clip(points);
Export.image.toDrive({
  image: clip,
  description: 'Cloudfreecomposite',
  scale: 30,
  region: judet,
  crs : 'EPSG:3857'
});
//Map.addLayer(clip,{bands: ['B4', 'B3', 'B2'], max: 128},
//'Cloud free composite diplayed in natural colors');

// Compute the Normalized Difference Vegetation Index (NDVI).
var nir = clip.select('B4');
var red = clip.select('B3');
var ndvi = nir.subtract(red).divide(nir.add(red)).rename('NDVI');
// Display the result.
var ndviParams = {min: -1, max: 1};
Map.addLayer(ndvi, ndviParams, 'NDVI image');
Export.image.toDrive({
  image: ndvi,
  description: 'CloudfreeNDVIcomposite',
  scale: 30,
  region: judet,
  crs : 'EPSG:3857'
});

//Create median filter. To conserve the edges.
var median = ndvi.focal_median({radius:4});
Export.image.toDrive({
  image: median,
  description: 'Medianfilter',
  scale: 30,
  region: judet,
```

```
  crs : 'EPSG:3857'
});

// Define two kernels to build a high-pass filter (enhance edges)
// Create a list of weights for a 3x3 kernel to avoid losing information.
var list = [0, 0, 0];
print(list);

// The center of the kernel is one.
var centerList = [0, 1, 0];
print(centerList);

// Assemble a list of lists: the 3x3 kernel weights as a 2-D matrix.
var lists = [list, centerList, list];

// Create the kernel from the weights.
var kernel = ee.Kernel.fixed({width :3, height : 3, weights : lists, normalize :true});
print(kernel);
print(lists);

// Define a Laplacian kernel added with the kernel created previously
var laplacian = ee.Kernel.laplacian8(8);
var add = kernel.add(laplacian);
print(add);

// Convolve the noise-free image with the high pass filter
var segmentation = median.convolve(add).zeroCrossing();
print('Segmentation',segmentation);
Export.image.toDrive({
  image: segmentation,
  description: 'Segmentation',
  scale: 30,
  region: judet,
  crs : 'EPSG:3857'
});

//invert 0 and 1 in the image
var invert=segmentation.not();

// Define a kernel to build a structuring element for a morphological operation
var kernel1 = ee.Kernel.square({radius: 3});
var kernel2 = ee.Kernel.square({radius: 2});

// Perform an dilatation
var dilatation = invert
          .focal_min({kernel: kernel1, iterations: 1});

//Perfom an erosion
var erosion = dilatation.focal_max({kernel: kernel2, iterations: 1});
print('Closing',erosion);
```

```
Map.addLayer(erosion,{},'Morphological closing');
Export.image.toDrive({
  image: erosion,
  description: 'Morphological closing',
  scale: 30,
  region: judet,
  crs : 'EPSG:3857'
});

// Reduce the image obtained from morphological operation into multiple vectors
var vectors = erosion.reduceToVectors({
  geometry: judet,
  geometryType : 'polygon',
  eightConnected: false,
  bestEffort :true,
  scale : 30
});

// Remove the edges to only keep inside of the crops. Edges = 0 crops = 1
var crops = vectors.filter(ee.Filter.eq('label',1));
var test  = crops.limit(1);
var ndwiViz = {min: 0.5, max: 1, palette: ['#B0F2B6']};
Map.addLayer(crops, ndwiViz, 'Crops', false);


// Create a function that compute the area in km2 directly from the feature's
geometry.
var Area = function(feature) {
return feature.set({areakm: feature.area(1).divide(1000*1000)});
};

// Compute the surface for each vectors and get a number
var csurface = ee.Number(crops
    .map(Area));
Export.table.toDrive({
collection: csurface,
description: 'Area',
fileFormat: 'CSV'
});

// Visual check
//
// Limit to the first crop of the feature collection
var first = crops.limit(1);
print('First',first);
// Compute the surface
var surface = ee.Number(first
    .map(Area));
print('Suface in km2', surface);
// Draw the crop
```

```
var visualC = first.map(Area);
// Display the crop clipped with ndvi layer
var clipC = ndvi.clip(visualC);
var ndwiViz = {min: 0.5, max: 1, palette: ['00FFFF', '0000FF']};
Map.addLayer(clipC, ndwiViz, 'Visual check', false);
```

2. Matlab code used to compute histograms

```
close all, clear;home
D=xlsread('Ba.xlsx');
%% extract data for each year
A_2006=D(:,2);
A_2010=D(:,4);
A_2016=D(:,6);

%% remove small areas and too large areas
minsize = 2;
maxsize = 500;
A_2006(A_2006<minsize)= nan;
A_2006(A_2006>maxsize)=nan;
A_2010(A_2010<minsize)= nan;
A_2010(A_2010>maxsize)=nan;
A_2016(A_2016<minsize)= nan;
A_2016(A_2016>maxsize)=nan;

% look at the total area for each year
disp('total area')
sum(A_2006(isfinite(A_2006)))
sum(A_2010(isfinite(A_2010)))
sum(A_2016(isfinite(A_2016)))

% look at the number of fields for each year
disp('total nb fields')
sum((isfinite(A_2006)))
sum((isfinite(A_2010)))
sum((isfinite(A_2016)))

%% Create a Matrix with those data
z =[A_2006, A_2010, A_2016];
z(z == 0) = NaN;
%% Create bins or do it randomly
xbins = [20 100];
[y, b] = hist(z);
%% Display figure
figure(1);
hold on
bar(b,y,'grouped');
xlabel ('Surface in hectare','FontWeight','bold')
ylabel('Log Frequency','FontWeight','bold')
legend ('2006','2010','2016')
```